Study on Omega Signals Observed by Poynting Flux Analyzer on board the Akebono Satellite

Dissertation

Study on Omega Signals Observed by Poynting Flux Analyzer on board the Akebono Satellite

Graduate School of
Natural Science & Technology
Kanazawa University

Division of
Electrical Engineering and
Computer Science

Student ID No. 1323112011
Name : I Made Agus Dwi Suarjaya
Chief Advisor : Yoshiya Kasahara
March 21, 2017

Preface

The Akebono satellite was launched in 1989 to observe the Earth's magnetosphere and plasmasphere. Omega was a navigation system with eight ground station transmitters and a transmission pattern repeating every 10 s. From 1989 to 1997, the Poynting Flux Analyzer (PFX) on board the Akebono satellite received signals at 10.2 kHz from these stations. The huge amounts of PFX data are valuable for studying the propagation characteristics of very-low-frequency waves in the ionosphere and plasmasphere. In this study, we developed a method for automatic detection of Omega signals from the PFX data in a systematic way: the method involves identifying a transmission station, calculating the delay time, and estimating the signal intensity. We demonstrate the reliability of the automatic detection system with which we were able to detect the Omega signals and showed that the signals propagate to the opposite hemisphere along the Earth's magnetic field lines. For eight years (96 months) from October 1989 to September 1997, we detected 127,900 and 476,134 signals in the PFX magnetic and electric field data, respectively, and demonstrated that the proposed method is sufficiently powerful for statistical analyses.

We study the propagation patterns of Omega signals to understand the propagation characteristics that are strongly affected by plasmaspheric electron density and ambient magnetic field. We show unique propagation patterns of Omega signal transmitted from high–middle-latitude stations using the data captured by the PFX subsystem on board the Akebono satellite for about eight years from October 1989 to September 1997. We demonstrate that the signals transmitted from almost the same latitude in geomagnetic coordinates propagated

differently depending on the geographic latitude. We also study propagation characteristics as a function of local time, season and solar activity. The Omega signal tended to propagate farther on the nightside than on the dayside, and widely distributed during winter than summer. When solar activity was at a maximum, the Omega signal propagated at a lower intensity level; in contrast, when solar activity was at a minimum, the Omega signal propagated at a higher intensity level and farther from the transmitter station.

Table of Contents

List of Tables

List of Figures

Chapter 1
Introduction

1.1 Research Background

The Earth's plasmasphere is located at the inner part of the magnetosphere and is mainly filled with cold plasma. VLF waves such as whistlers (Carpenter, 1963) and Omega signal are strongly affected by the electron density profile. Major species of ions in the plasmasphere are protons, helium ions, and oxygen ions and composition ratio of these ions plays an important role in the propagation effect of VLF waves such as subprotonospheric whistler and magnestospherically reflected whistler (Kimura, 1966). Hence it is very important to clarify the spatial distribution of electron density as well as ion constituents in the magnetosphere to understand the propagation characteristics of VLF waves. In other words, propagation characteristics of the VLF wave could be an important clue to study the electron density profile in the magnetosphere.

Several studies to determine the electron density profile around the Earth had previously been conducted. Some studies of in situ satellite observations are capable of revealing the features of plasmasphere such as "notches" (Sandel et al., 2001; Sandel et al., 2003). Particular long-lived (2–3 days) depleted region (MLT>1.5–2 hours) or "notch" was extended out from L ~ 3 in the plasmasphere (Kotova et al., 2014). Remote sensing by using ground-based magnetometers enabled us to compare mass density and electron density between different L-Shell by using multiple observation station along the 330° magnetic longitude,

spanning L-Shell between 1.5 and 3.4 (Chi et al., 2013). Is was also demonstrated that mass density can decrease within a few hours by 50% or more 0.5 RE or further inward of the plasmapause especially during disturbed times (Menk et al., 2014), where RE is the radius of the Earth. Determination of electron density by using the measurement data of electromagnetic waves is also important, including research on the dispersion of electromagnetic waves originating from lighting discharge, known as lightning whistlers (Helliwell, 1965), because the propagation velocity of whistler-mode waves is dependent on the electron density profile around the Earth (Crouchley, 1964; Singh et al., 2003). Statistical studies of lightning whistlers have been performed using ground observatory data at Tihany, Hungary (Tarcsai et al., 1988; Collier et al., 2006; Lichtenberger et al., 2008). Another statistical study of lightning whistlers was carried out using the Akebono satellite (Oike et al., 2014). These studies have provided information on the absorption effect of lightning whistlers in the ionosphere.

Because the global plasmaspheric electron density changes day by day, it is important to assess the trend of this change using statistical study of electromagnetic wave propagation over several years. In addition, observing signals from artificial transmitters are worth analyzing for such a purpose because these transmitters were constantly transmitting signals with constant power; thus, it is possible to analyze the extent of change in the wave propagation. This technique has been used to estimate the ionospheric topside and bottom-side profile with sounder (Reinisch et al., 2001; Ganguly et al., 2001) which is capable to check the ionospheric peak parameters such as density, height and peak shape (Pulinets et al., 2001).

Japan has launched a satellite nicknamed Akebono (EXOS-D) in 1989 to observe the Earth's magnetosphere and plasmasphere. The satellite consists of several scientific instruments such as particle detectors, magnetometer, electric field detector, plasma wave instruments and auroral camera. The VLF instrument

is one of the instruments on board Akebono to measure VLF plasma waves and the Poynting flux Analyzer subsystem (PFX) is a subsystem of the VLF instrument (Kimura et al., 1990). The PFX is a waveform receiver that measures three components of magnetic fields and two components of electric fields. The waveforms generated from the PFX have band-width of 50 Hz at fixed center frequency from 100 Hz to 12.75 kHz. The Wide Dynamic Range Amplifier (WIDA) hybrid ICs are equipped for the gain control to achieve wide measurable dynamic range (Kimura et al., 1990).

Omega system was a navigation system to provide a navigational aid for domestic aviation and oceanic shipping with 8 ground station transmitter located at Norway, Liberia, Hawaii, North Dakota, La Reunion Island, Argentina, Australia, and Japan (Morris et al., 1994). The PFX had been observed Omega signals transmitted from these 8 ground stations around 1989-1997. The PFX captured one of the common frequency of Omega signal, that is the 10.2 kHz. Later on, this navigation system was shut down in 1997 in favor of the GPS system.

Omega signal data captured by the PFX on board the Akebono have been used to estimate the global plasmaspheric electron density deduced from in situ electron density and wave normal directions (Sawada et al., 1993). In particular, a tomographic electron density profile could be determined by calculating the Omega signal propagation path using a ray-tracing method. This method could estimate the propagation path using 1-h data of single satellite observation (Kimura et al., 2001). The algorithm was further improved with a flexible method and novel stochastic algorithm. This enabled separate estimation of the effects of the ionosphere and plasmasphere (Goto et al., 2003).

Because the transmission pattern of frequency, the time, and the location of each station is known, we can easily distinguish the signal source. We can then determine many propagation properties such as attenuation ratio, propagation

direction, propagation time (delay time) from the transmission station, and the observation point along the satellite trajectories. Such parameters depend strongly on the plasma parameters along the propagation path. Therefore, it is valuable to analyze such propagation characteristics of VLF waves in the ionosphere and plasmasphere statistically using the long-term observation data.

We investigate statistical features of the Omega signals detected by the PFX from 1989 to 1997. To achieve this purpose, we picked up Omega signals from the enormous amount of the PFX data using an automatic detection program developed by Suarjaya et al. (2016). The methods used are consist of FFT analyses, determination of the stations that transmitted the signals, estimation of delay time, discrimination of signal existence, and estimation of signal intensity. We also added some error detection and efficient processing methods for rapid analysis. The results for intensity, delay time, and local time-dependence analysis are presented as geographic and geomagnetic maps.

1.2 Akebono Satellite

1.2.1 Overview

The Akebono satellite was launched at 23:30 UT on February 21, 1989 in order to investigate energy flow from the magnetospheric tail to the auroral region. The Akebono satellite was tracked by four tracking stations at Kagoshima Space Center in Japan, Prince Albert Radar Laboratory in Canada, Esrange Space Center in Sweden, and Antarctic Syowa Station in Antarctica.

The satellite contains eight scientific instruments (Kasahara, 1995):

(a) EFD (electric field detectors)
(b) MGF (magnetic field detectors)
(c) VLF (very-low-frequency plasma wave detectors)
(d) PWS (plasma wave detectors in the high-frequency range and sounder experiments)

(e) LEP (low-energy particle spectra analyzer)

(f) SMS (super-thermal ion mass spectrometer)

(g) TED (temperature and energy distribution of plasma)

(h) ATV (auroral television camera)

1.2.2 VLF Instruments

The Akebono VLF instruments were designed to investigate the wave phenomena closely associated with energetic particle precipitation in the auroral zone, wave–particle interaction phenomena, and wave physics (Kimura et al., 1990). Figure 1.1 shows the configuration of wave sensors and coordinate systems of the Akebono satellite. The spin axis of the satellite was the Z axis, and was always directed toward the sun. The loop antennas were directed to the Y axis, the search coils were directed to the −Y axis, and the flux-gate magnetometers were directed to the −X axis. Two wire antennas were directed at 45° from the X and Y directions.

The VLF instruments of the Akebono consisted of five subsystems:

(a) PFX (wave normal and Poynting flux analyzer)

(b) MCA (multichannel analyzer)

(c) ELF (extra-low-frequency range analyzer)

(d) VIP (vector impedance probe)

(e) WBA (wide-band analyzer)

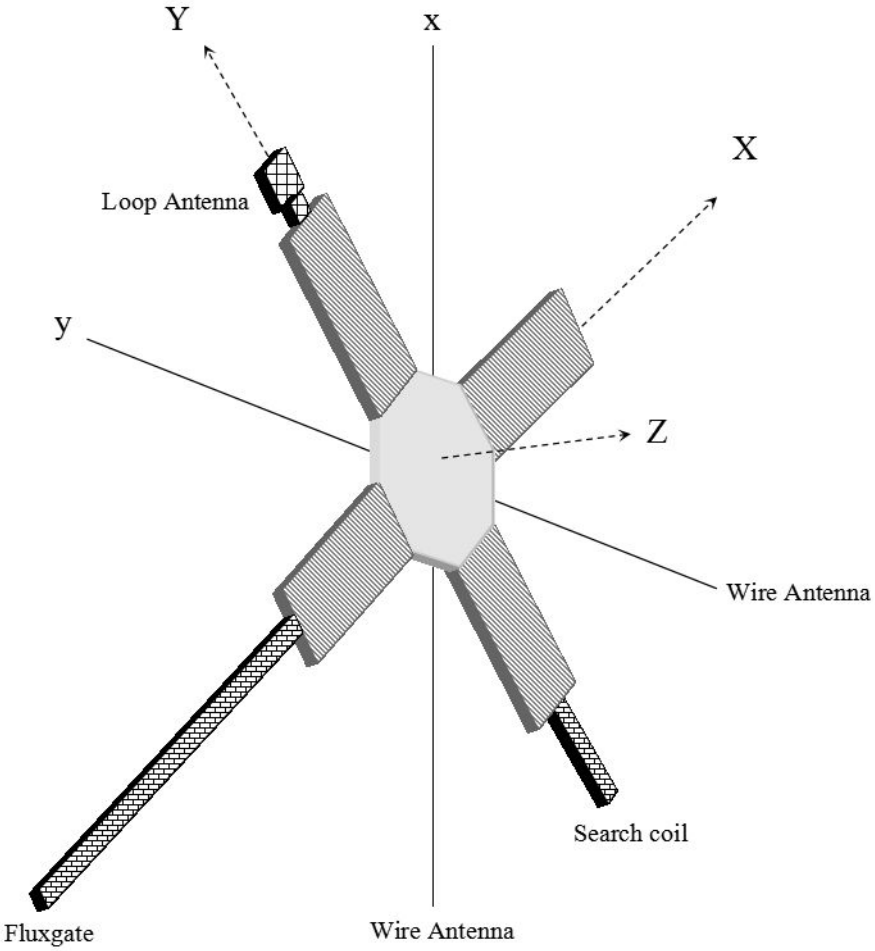

Figure 1.1 Configuration of wave sensors and coordinate systems of the Akebono satellite. The spin axis of the satellite was the Z axis and was always directed to the sun.

1.2.3 PFX Instrument

The PFX subsystem of the Akebono satellite measured three components of magnetic fields (B_1, B_2, and B_3) and two components of electric fields (E_x and E_y). The subsystem comprised five-channel triple-super-heterodyne receivers with an output bandwidth of 50 Hz. It also contained a local oscillator that could be stepped or fixed at a specific center frequency with a range of 100–12.75 kHz and was equipped with a Wide Dynamic Range Amplifier (WIDA) hybrid IC to control the gain in the dynamic range for more than 80 dB (Kimura et al., 1990).

The WIDA hybrid IC automatically checked the averaged signal level every 0.5 s and the gain of each channel could be changed independently in 25 dB steps from 0 dB up to 75 dB. For our study, we use B_X, B_Y, B_Z, E_X and E_Y in static coordinate system converted from B_1, B_2, B_3, E_x and E_y obtained in the antenna coordinate system fixed to the spinning satellite as defined in Kimura et al. (1990). The static coordinate system is referred to the direction of the geomagnetic field (the geomagnetic field line is in the X-Z plane and Y is perpendicular to the X-Z plane) and the direction of the sun (Z-axis).

1.2.4 PFX Data

To measure Omega signals, we selected and analyzed the PFX data when the center frequency was fixed at 10.2 kHz. The PFX data were recorded in the Common Data Format (CDF) developed by the National Space Science Data Center (NSSDC) at NASA. This ensured standardized read/write interfaces for multiple programming languages and software. The waveforms measured by the PFX were originally two components of the electric field in the spin plane and three components of the magnetic field in the B_1, B_2, and B_3 directions. These waveforms were orthogonal with respect to each other but different from the satellite coordinates. These waveforms were calibrated, converted into non-spinning satellite coordinates, and stored in the CDF files. One month of PFX data occupied 5–10 GB and one year of data consumed approximately 60–90 GB. In total, the amount of data from 1989 to 1997 is approximately 570 GB.

Table 1.1 shows the data structure of one record of PFX data inside a CDF file. Each record stored 500 ms of PFX data with 160 sample points each. Epoch contains Date and Time information in CDF file standard with four encoding format. Label_E consists of two arrays with values of E_X0. or E_Y0.. Label_B consists of two arrays with values of B_X0., B_Y0., or B_Z0.. Frequency stored the observation center frequency, which could be stepped or fixed: this frequency

was fixed at 10,200 Hz around the end of September 1989 to observe the Omega signal. E consists of 2 by 160 arrays that contain the electric field values. B consists of 3 by 160 arrays that contain the magnetic field values. PostGap stored the quality flag with possible values of 0 for normal, 1 for saturated data, or other for undefined.

Table 1.1 Data structure of one record of PFX data inside a CDF file. Each record stored 500 ms of PFX data with 160 sample points each.

Variables Name	Variables Type	Values
Epoch	EPOCH	14-DEC-1989 00:01:53.503
Label_E [2]	CHAR/5	E_X0.
Label_B [3]	CHAR/5	B_X0.
Frequency	UINT4	10200
E [2][160]	FLOAT	0.00000072342345432123
B [3][160]	FLOAT	0.00000000000045432123
PostGap	UINT4	0

Figure 1.2 shows the 10 s raw waveform of the PFX data at 18:05:29.503 UT on December 14, 1989. In the figure, we can observe the raised intensity from 18:05:33.500 UT to 18:05:34.900 UT, which in this case is the Omega signal from the Australia station. In the electric field components of E_X and E_Y from 18:05:33.800 UT to 18:05:34.300 UT, the PFX receivers both for E_X and E_Y were saturated as indicated by the red arrows, because an intense Omega signal was captured. But the gain of these channels was immediately adopted adequately at 18:05:33.800 UT thanks to the WIDA IC. The WIDA IC worked independently for each five components. Therefore, all channels are not necessarily saturated but some components of the magnetic and/or electric field were occasionally saturated. During the period of saturation, signal intensity is apparently clipped and we cannot estimate absolute intensity. Then we define 'raise time' of Omega signal at the beginning point of the signal, while we use the data 0.5 seconds after the raise time when we evaluate 'absolute intensity' of the signals to exclude the saturated

data. The detailed detection algorithm to derive raise time and intensity is described in chapter 2.

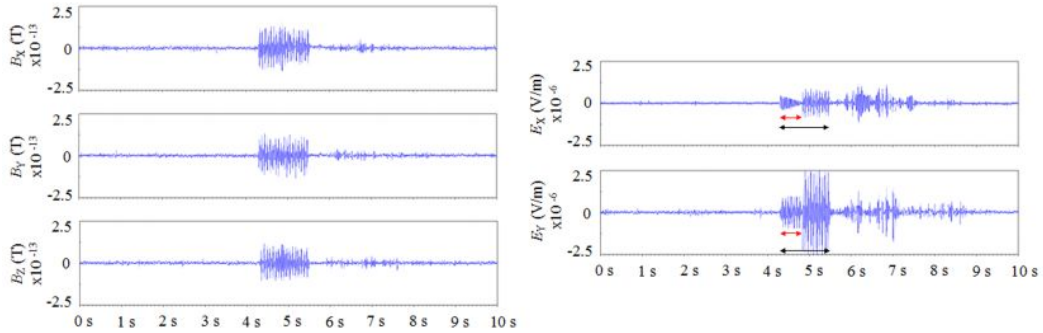

Figure 1.2 Raw PFX waveform at 18:05:29.504 UT on December 14, 1989. There is a raised intensity from 18:05:33.500 UT to 18:05:34.900 UT, which in this case is the Omega signal from the Australia station.

1.3 Omega System

1.3.1 Overview

The Omega signal is a VLF signal between 10 and 14 kHz transmitted by the Omega navigation system that was operational in 1971. Before the system was shut down in 1997, its purpose was to provide a navigational aid for domestic aviation and oceanic shipping. The Omega receiver determined a location based on the phase of the signal from two or more of the Omega stations (Morris et al., 1994). This Omega signal was transmitted from eight ground stations with each station transmitting a unique pattern, on the basis of which our analyzer software could determine the source of the signal.

1.3.2 Transmission Stations and Pattern

Figure 1.3 shows the location of the eight transmitter stations of the Omega system. The strategic locations of the stations ensured coverage of most Earth regions and the receiver could receive signals from at least three stations with an

accuracy of 5–10 km. The location of these Omega stations were Norway (NW), Liberia (LB), Hawaii (HW), North Dakota (ND), La Reunion Island (LR), Argentina (AZ), Australia (AS), and Japan (JP).

The transmission pattern from each station is shown in Figure 1.4. There are four common frequencies of the Omega signal (10.2, 13.6, 11.33, and 11.05 kHz) with one unique frequency for each station. Each station transmitted the common frequencies signal with different timing, with one transmission in each 10-s interval. The unique frequency of each station was transmitted four times in each 10-s interval. There was an interval of 0.2 s separating each of the eight transmissions, with variations in the duration for each station.

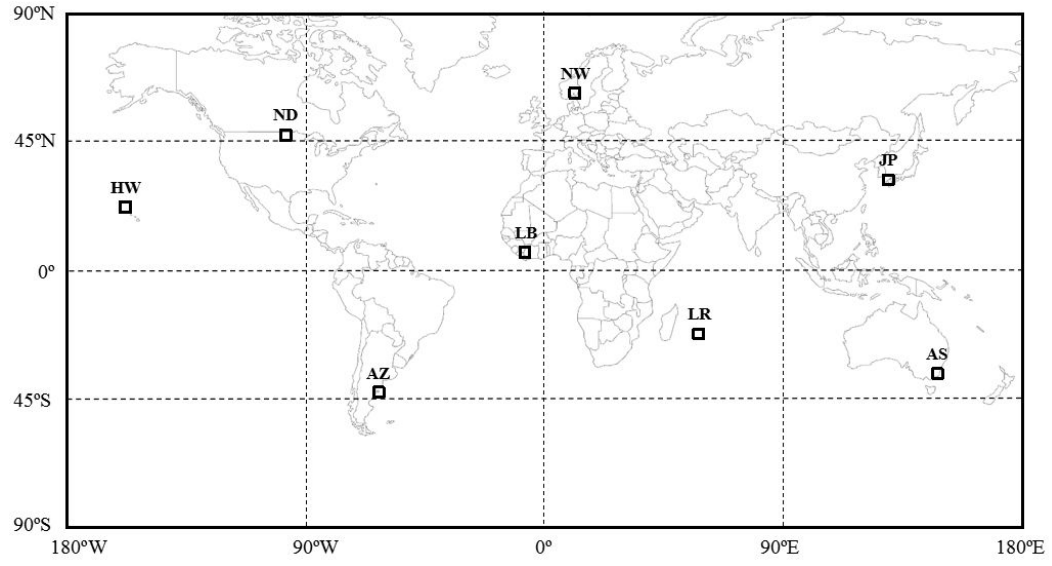

Figure 1.3 Omega System transmitter station locations. The locations of these Omega stations were Norway (NW), Liberia (LB), Hawaii (HW), North Dakota (ND), La Reunion Island (LR), Argentina (AZ), Australia (AS), and Japan (JP).

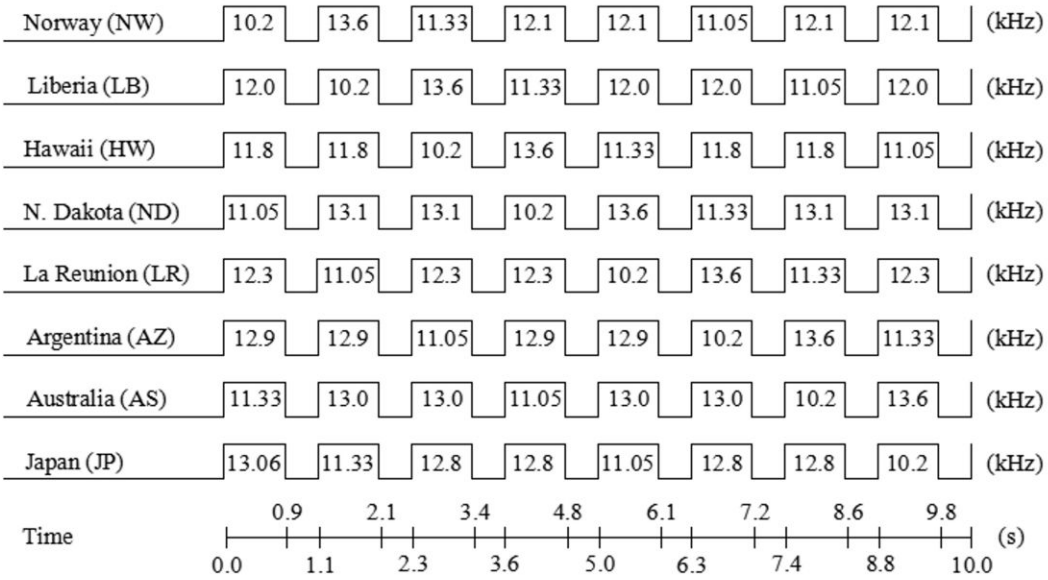

Figure 1.4 Transmission pattern of the Omega System. Each station transmitted four common frequencies and one unique frequency in each 10-s interval.

1.4 Purpose of the Present Work

Manual processing of all the data from 1989 to 1997 will take a large amount of time. Furthermore, additional processes and analyses will be required to obtain different results such as analysis based on magnetic local time, seasonal propagation analysis, and yearly propagation analysis. Our automatic detection method makes all of the analytical processes simpler and is able to produce most of the required results faster and more efficiently than manual processing. Herein, we discuss automatic detection methods for faster analysis of huge amounts of PFX data to study the propagation characteristics of VLF waves, which, in this case, is the Omega signal.

Global plasmaspheric electron density changes day by day: it is important to detect the trends in this change by statistical study of electromagnetic wave propagation for several years duration transmitted by artificial transmitters. Observing signals from artificial transmitters is necessary because these

transmitters were transmitting signals with constant power all the time; thus, we can analyze how much change to the propagation occurred.

1.5 Dissertation Organization

The present work is organized into six chapters.

In Chapter 1, we present the research background, an overview of the Akebono satellite, the VLF instruments equipped on the satellite, the PFX instrument as one of the VLF subsystems, the PFX data as the output of the PFX subsystem, an overview of the Omega System, the Omega system's transmission stations and pattern, and the purpose of this study.

In Chapter 2, we explain the automatic detection of the Omega signal using FFT analysis, then how to perform signal detection and threshold level determination, followed by delay time detection, signal discrimination, and intensity determination; in addition, we describe how error detection is handled.

In Chapter 3, we present an overview of our PFX Analyzer, the Akebono orbit data structure, and some features of the PFX analyzer such as the real-time data analysis capabilities, CSV files and results view, and saving and loading Map files.

In Chapter 4, we present the results of propagation analysis of the Omega signal, first by using one event study of the Akebono trajectory, followed by analysis of high–middle-latitude stations, analysis based on magnetic local time (MLT), analysis based on seasonal propagation, and finally an analysis based on yearly propagation in connection with solar activity.

In Chapter 5, we present results and discussion of the differences between the magnetic and electric fields, as well as all-station intensity maps and delay time maps that display interesting patterns related to the global electron density.

Finally, in Chapter 6, we summarize the results presented in Chapters 2–5 and conclude the present work.

Chapter 2
Automatic Detection of Omega Signal

2.1 Overview

To analyze these Omega signals, we are using automatic detection methods such as FFT analyses, determination of the stations which transmitted the signals, estimation of delay time, discrimination of signal existence and estimation of signal intensity. We also added some error detection and efficient processing method for fast analyzing.

2.2 FFT Analysis

The PFX data is stored as waveforms sampled at rate of 320 Hz. For FFT analysis, we used FFT size of 32. Therefore, the time resolution was 100 ms and the frequency resolution was 10 Hz. To improve the accuracy of delay time detection, we applied an overlap-add FFT that moves every three sample points for a higher time resolution (~9.4 ms) when the first signal was detected. Although PFX measured only two components of the electric field, we could derive another component (E_Z) if we assumed the measured signal as a single plane wave (Yamamoto et al., 1991). This is expressed using equation (2.1).

$$E_Z = -\frac{E_X B_X + E_Y B_Y}{B_Z} \tag{2.1}$$

After we calculated the E_Z component, we could use it to calculate the absolute intensity of the electric field $|E|$ as shown in equation (2.2). In the same way, we also calculated the absolute intensity of the magnetic field $|B|$ using equation (2.3). We use dB (V/m) for the electric field measurement unit and dB (T) for the magnetic field measurement unit.

$$|E| = \sqrt{E_X^{\,2} + E_Y^{\,2} + E_Z^{\,2}} \tag{2.2}$$

$$|B| = \sqrt{B_X^{\,2} + B_Y^{\,2} + B_Z^{\,2}} \tag{2.3}$$

2.3 Signal Detection and Threshold Level Determination

We first estimated the raise time of each signal by comparing the average intensity of specific time frame to the threshold level, expecting a sudden increase in intensity. Second, we determined the transmission station by comparing the raise time with the transmission patterns of the eight Omega stations as shown in Figure 2.1. At 0000 UT on January 1, 1972, the Omega and UTC scales were identical. However, we subsequently had to conduct a leap seconds calculation to synchronize the omega time and UTC because the Omega had no leap seconds like the UTC (Morris et al., 1994). On December 31, 1989, the Omega time led the UTC by 14 s.

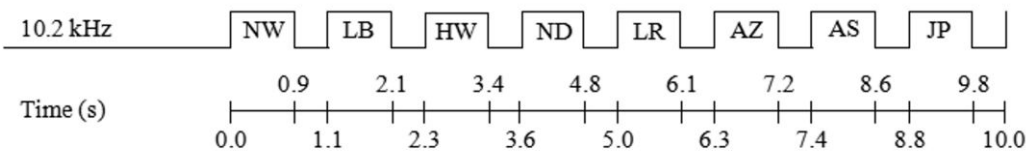

Figure 2.1 Transmission Pattern of the 10.2 kHz Omega Signal. There is an interval of 0.2 s separating each of the eight transmissions, with variations in the duration for each station.

The threshold level we use in the detection method, is based on the comparison of ambient noise level and Omega signal intensity. In Figure 2.2, we show parameters for the comparison of ambient noise and Omega signal intensity visualized on a spectrogram of 10 s of PFX data in the magnetic field (a) and in the electric field (b) beginning at 18:05:29.503 UT on December 14, 1989 when the Omega signal from Australia and Japan were expected to be received. The spectrogram in Figure 2.2 consists of 16 bins in frequency (Δf = 10Hz/bin) and 1057 bins in time (Δt = ~9.4ms/bin). We separated it into three frequency area bins, where P_c denotes the center frequency (consisting of 5 bins in frequency and 1 bin in time), P_u denotes the upper frequency (consisting of 5 bins in frequency and 1 bin in time), and P_l denotes the lower frequency (consisting of 6 bins in frequency and 1 bin in time).

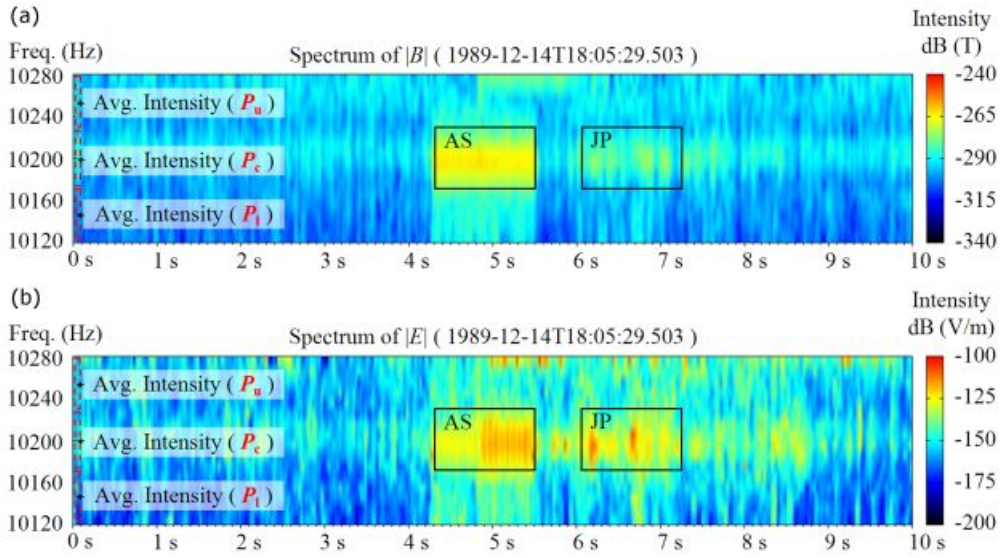

Figure 2.2 Spectrum of the Magnetic Field at 18:05:29.503 UT on December 14, 1989. We separated it into three frequency area bins (P_c, P_u, and P_l) to compare ambient noise and Omega signal intensity in the magnetic field (a) and in the electric field (b).

Based on extracted data from the analyzer, Figure 2.3 compares ambient noise and Omega signal intensity in the magnetic field at 18:05:29.503 UT on December 14, 1989. We can see the raised intensity level on P_c compared with P_u

and P_l. This raised intensity level occurred within the expected transmission time of the Australia station (from approximately 18:05:33.700 UT to 18:05:34.900 UT) and the Japan station (from approximately 18:05:35.500 UT to 18:05:36.500 UT).

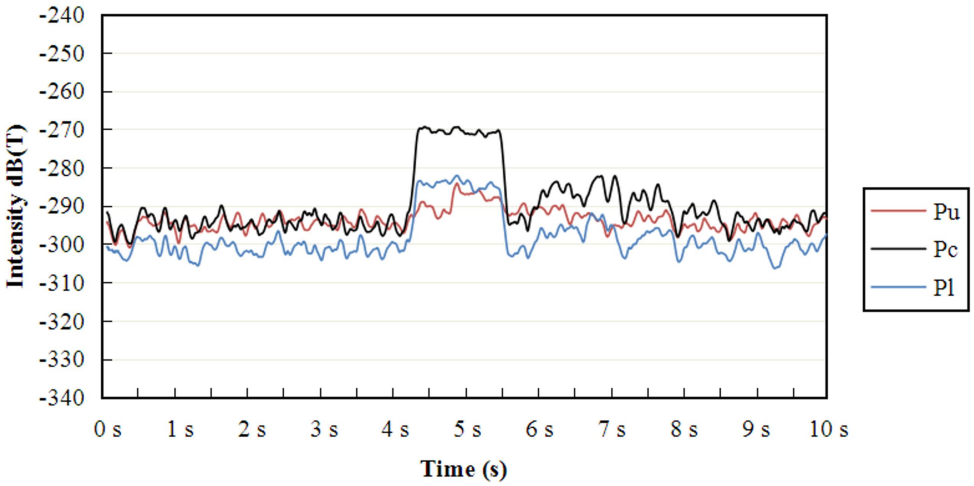

Figure 2.3 Comparison of Omega Signal Intensity and Ambient Noise Level in the Magnetic Field. Raised intensity level occurred within the expected transmission time of the Australia station (from approximately 18:05:33.700 UT to 18:05:34.900 UT) and the Japan station (from approximately 18:05:35.500 UT to 18:05:36.500 UT).

A comparison of ambient noise and omega signal intensity in the electric field can be seen in Figure 2.4, which is based on extracted data from the analyzer at 18:05:29.503 UT on December 14, 1989. In this case, the signal was saturated from approximately 18:05:33.800 UT to 18:05:34.300 UT because the WIDA IC was controlling the gain of receiver. In this case, we need to calculate the intensity of the saturated signal after 0.5 s. We recognized this saturation by calculating and comparing each each signals for any sudden change in the intensity of the constant duration. In this case, the WIDA IC will affect the next 0.5 s sample for increased gain when activated. This type of saturated signal could affect any of the 5 components measured by the PFX subsystem because the WIDA IC works independently for each component.

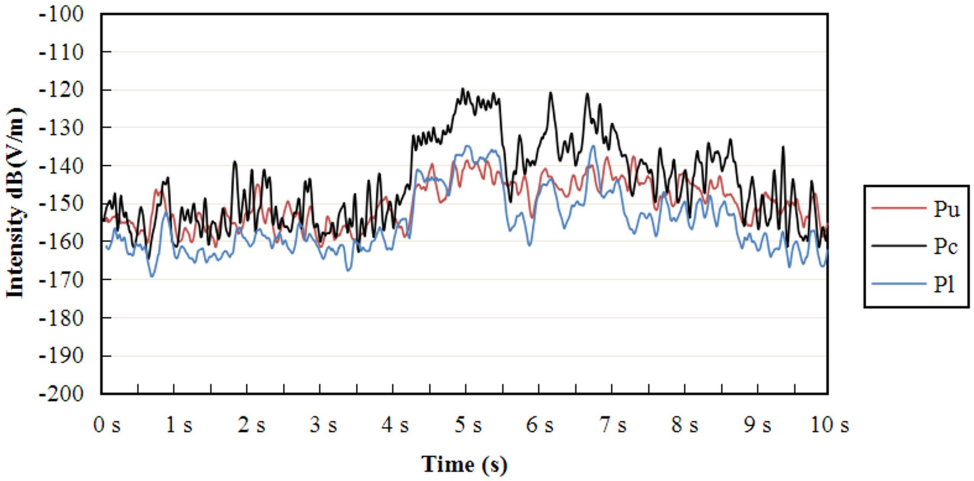

Figure 2.4 Comparison of Omega Signal Intensity and Ambient Noise Level in the Electric Field. The signal was saturated from approximately 18:05:33.800 UT to 18:05:34.300 UT because the WIDA IC was controlling the gain of receiver.

2.4 Delay Time Detection

We calculated the delay time of the signal by detecting the raise time of intensity and compare it with surrounding frequency from start time transmission during each station transmission duration as shown in Equation (2.4).

$$t_d = \begin{cases} t_n - t_0 & \text{if } \left(P\_u_{\mathrm{n}} + P\_l_{\mathrm{n}}\right)/2 + T_{\mathrm{P}} < P_n \text{ and } \left(P_n - P_{n-1}\right) > T_P \\ 0 & \text{otherwise} \end{cases} \tag{2.4}$$

where T_{P} denotes the intensity threshold (8 dB), t_{d} denotes delay time in seconds, P_{n} denotes intensity strength of center frequency consists of 5 bins in frequency (Δf = 10Hz/bin) and 20 bins in time (Δt = ~9.4ms/bin), P_u_{n} denotes intensity strength of upper frequency consists of 5 bins in frequency (Δf = 10Hz/bin) and 20 bins in time (Δt = ~9.4ms/bin), P_l_{n} denotes intensity strength of lower frequency consists of 5 bins in frequency (Δf = 10Hz/bin) and 20 bins in time (Δt = ~9.4ms/bin), t_0 denotes start time of the station's transmission, t_{n} denotes start

time of P_n, and n denotes the iteration number for every 1 bin in time (Δt = ~9.4ms/bin). In Figure 2.5, we show the parameters used for the delay time detection visualized on a spectrogram of 10 s of PFX data in the magnetic field start at 18:05:29.503 UT on December 14, 1989, when the Omega signal from Australia and Japan were expected to be received.

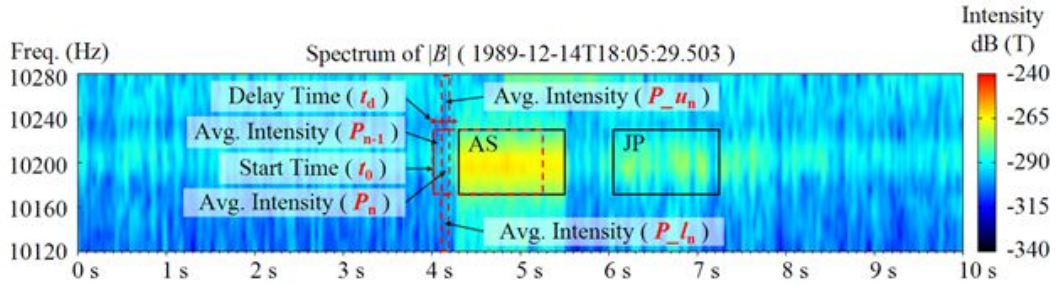

Figure 2.5 Parameters used in the Delay Time Detection Method. Delay time (t_d) calculated by detecting the raise time of intensity (P_n) and compare it with surrounding frequency (P_u_n and P_l_n) from start time transmission (t_0) during duration time of each station.

2.5 Signal Discrimination and Intensity Determination

In the next step, we determined signal existence by comparing the intensity of the expected duration of the Omega signal with the surrounding intensity (higher and lower frequency points of the center frequency). We determined signal existence and derived the signal intensity ($P_{\omega s}$) by using Equation (2.5)

$$P_{\omega s} = \begin{cases} P_s & \text{if } (P_a + P_b)/2 + T_P < P_s \text{ and } (P_w + T_w) < P_s \\ 0 & \text{otherwise} \end{cases} \qquad (2.5)$$

where P_a denotes the intensity strength of the upper frequency bins in decibels, P_b denotes the intensity strength of lower frequency bins in decibels, P_s denotes the intensity strength of center frequency bins in decibels. P_a, P_b, and P_s consists of 5 bins in frequency (Δf = 10Hz/bin) and variation (128 bins for Australia and 106 bins for Japan) of bins in time (Δt = ~9.4ms/bin) depends on the duration of the

Omega signal for each station. P_w denotes intensity strength of 16 bins in frequency (Δf = 10Hz/bin) and 1057 bins in time (Δt = ~9.4ms/bin) for every 10 s duration (1 window) in decibels.

In Figure 2.6, we show the parameters used for the calculation of the signal visualized on the same spectrogram as shown in Figure 2.5. In Figure 2.6, for example, P_s has total of 640 bins (5 bins in frequency and 128 bins in time) because the Omega signal from Australia station has 1.2 s in duration and we used overlap-add FFT. We defined two intensity thresholds T_P and T_W, where T_P had a fixed value of 8 dB and T_W had a fixed value of 5 dB.

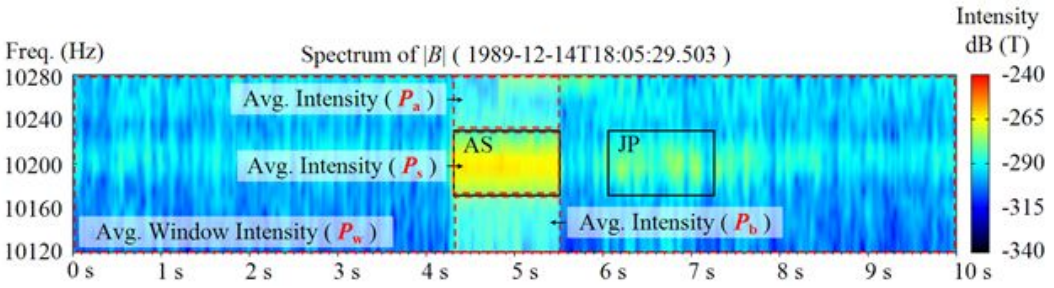

Figure 2.6 Parameters used for Discrimination and Intensity Calculations. The signal existence determined by comparing the average intensity of the expected duration of the Omega signal (P_s) with the surrounding frequency (P_a and P_b) and the ambient noise of 10 seconds duration or 1 window (P_w).

2.6 Error Detection Handler

For accurate results, we also applied error detection handling and a data smoothing process. It is possible for the analyzer to detect a high intensity noise as Omega signal. To handle this type of error detection, we applied a function that ignores a signal that is not detected continuously for a specific duration of time. This is currently set at 40 s. For example, when the signal is only detected for the first 30 s and then disappears in the next 10 s, the analyzer will ignore the signal and decide there is no signal detected for the entire 40 s. This handling occurs in

the background of the analyzer software and the analyzer will still show a rectangle that represent the detected signal.

We also applied a time smoothing algorithm to handle sudden peaks of delay time that may reflect false detection. This was accomplished by using moving average over the delay time data. We expect to obtain more reliable result using improved detection data.

Chapter 3
PFX Analyzer

3.1 Overview

We developed software to analyze the Omega signal data measured by the Akebono satellite from 1989 to 1997. The software was written in the Java programming language, and enabled us to detect Omega signals automatically for several months or years and then display the results of electric and magnetic intensity and delay time for specific locations of longitude, latitude, and altitude on geomagnetic and geographic maps of the Earth. Analyses of local time dependence are also available. An overview of the analyzer software is shown in Figure 3.1.

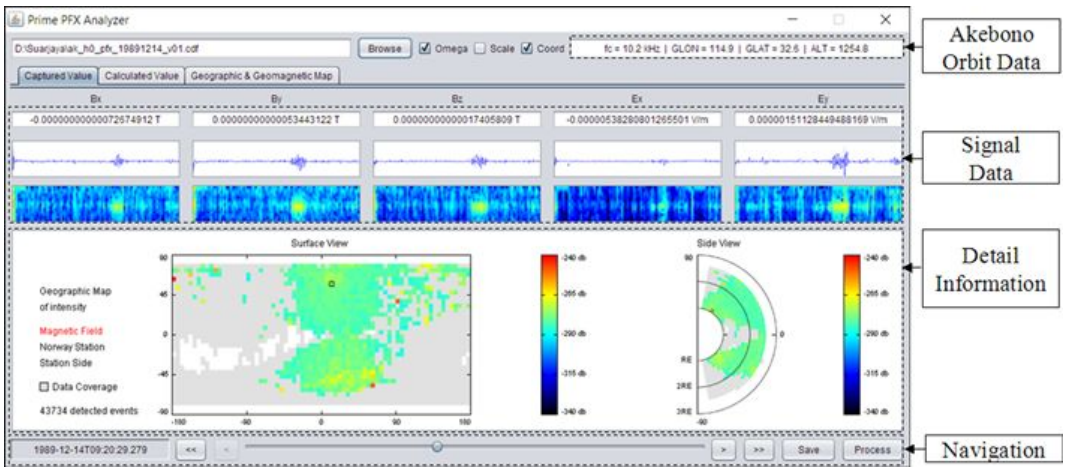

Figure 3.1 Overview of the PFX Analyzer, written in the Java programming language. The software enables automatic detection of Omega signals for several months.

This analyzer connects to the Akebono orbit database and can be used for manual analysis of each signal in real time by manipulating the navigation panel. Automatic analysis of the CDF files for one month of data requires 6–9 h of processing time using an Intel Quad Core with a 3.324 GHz CPU and 4 GB of memory. The computational time depends on the number of available signal data and data size. Depending on the computer specifications, it is possible to run multiple instances of the analyzer to speed up the process.

3.2 Akebono Orbit Data

The Akebono orbit data are stored in a relational database management system, PostGreSQL, running on Linux platforms. Table 3.1 shows the attributes and description of the orbit data. The database contains tables for each year. The attribute id indicates the time index with a value calculated based on converted date and time of the observation time into the total number of seconds in a specific year. The attribute alt contains information on the observation point altitude in kilometers. The attribute glat contains latitude information in geographic coordinates; glon contains longitude information in geographic coordinates; mlat contains magnetic latitude information of the observation point; and mlt contains magnetic local time information of the observation point. The attribute flat contains information on the latitude footprint at an altitude of 120 km along the magnetic field line from the satellite location. The attribute ilat contains information of invariant latitude. The attribute x,y,z stores the distance in kilometers from the center of the Earth in the geocentric coordinate system. The PFX analyzer fetches only id, alt, glat, glon, mlt, and ilat attributes for the analytical process.

The Akebono orbit data are automatically fetched from the database every 10 s of PFX data and displayed in the analyzer interface as shown in Figure 3.2. Only three attributes are shown in the analyzer: glon, glat, and alt. When no connection

is available, it is possible to disable this automatic process by turning off the coord radio button to the left of the label window. The fc value is the center frequency of the PFX taken from the PFX data in the CDF files.

Table 3.1 Akebono orbit data.

Attribute Name	Description
Id	Time index
Alt	Altitude
Glat	Latitude
Glon	Longitude
Mlat	Magnetic latitude
Mlt	Magnetic local time
Flat	Latitude of footprints
Ilat	Invariant latitude
x, y, z	Distance from the center of Earth

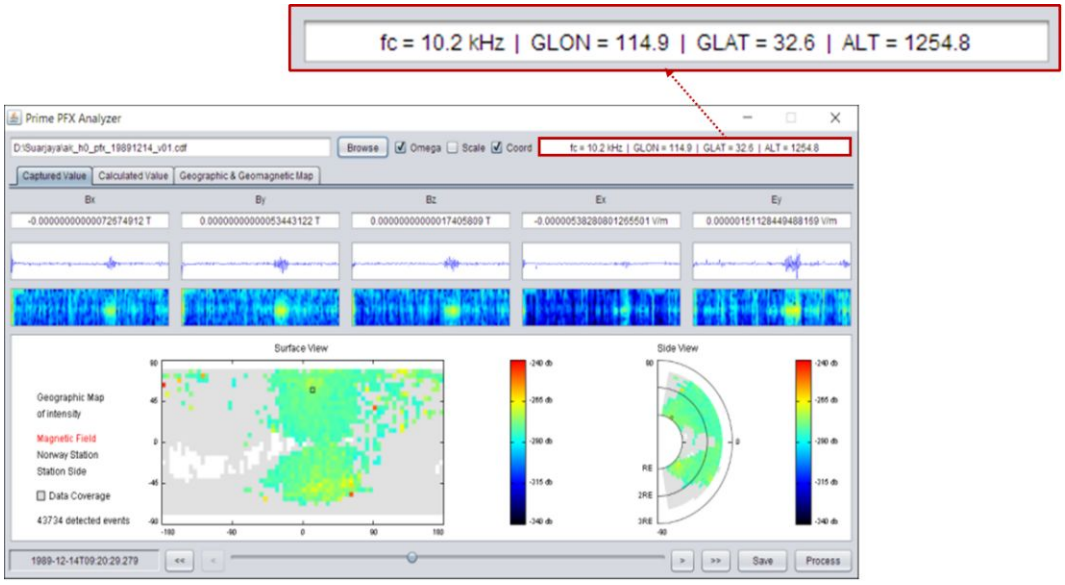

Figure 3.2 Akebono orbit data automatically fetched from the database for every 10 s of PFX data and displayed in the analyzer interface.

3.3 Features of the PFX Analyzer

3.3.1 Real-time Data Analysis

The PFX analyzer performs FFT analysis for every 10 s of PFX data (1 window). In Figure 3.3, the topmost label window shows values of each sample points inside the PFX data; by using single arrows (< or >) in the navigation control, users can view each of these sample points in real time. The middle plot window shows the raw waveform of the PFX data and the bottom plot window shows the spectrum of 10-s duration of the PFX data. This first tab window shows five components captured by the PFX.

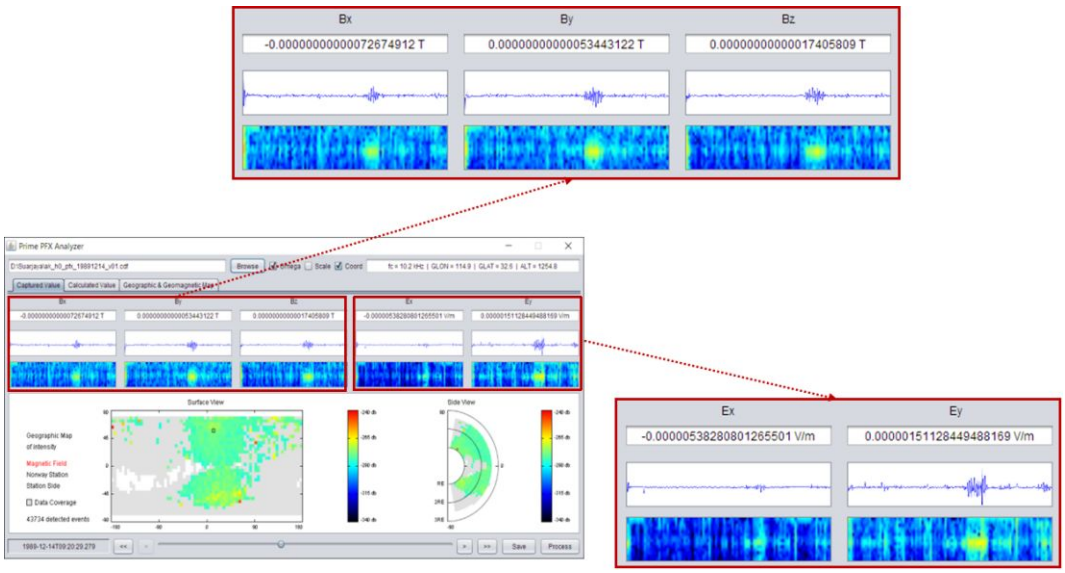

Figure 3.3 Five captured components (B_X, B_Y, B_Z, E_X, and E_Y) of the PFX data shown for real-time data analysis.

The second tab window of the PFX analyzer displays the other three calculated components of the PFX data, as illustrated in Figure 3.4. This window does not show sample points and raw waveforms because the calculated components do not have sample points and raw waveform data, as explained in the previous chapter.

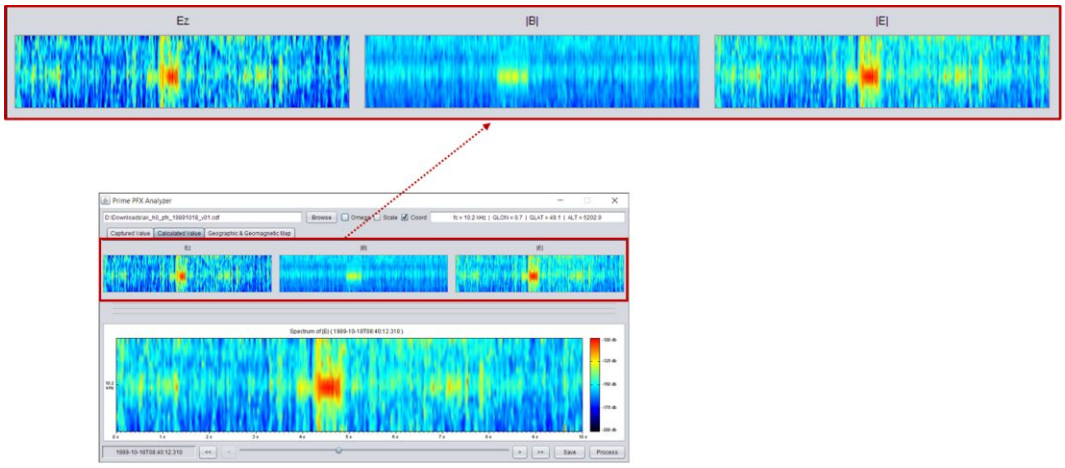

Figure 3.4 Three calculated components (EZ, |B|, and |E|) of the PFX data shown for real-time data analysis.

Figure 3.5 shows the detailed information window and navigation control of the PFX analyzer. Users can obtain detailed information in a specific window, such as the waveform, spectrum, and map windows in each tab. The leftmost window shows the epoch of the CDF files. The arrow buttons (< and >) are used to navigate through the sample points of the five captured components. Double-arrow buttons (<< and >>) are used to navigate every 10 s of the PFX data. The save button is used to save the detailed information into image files (PNG format). The process button is used to start the automatic detection process of the PFX analyzer.

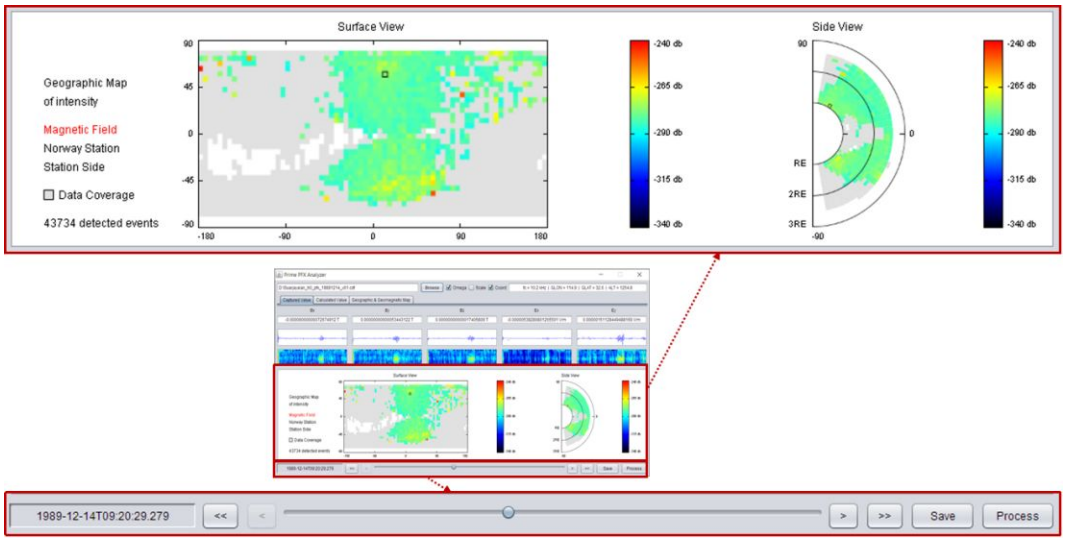

Figure 3.5 Detailed information of the selected components or selected results of the PFX data. The illustrated example shows real-time PFX data analysis.

3.3.2 CSV Files and Results View

The PFX analyzer will create CSV files during the automatic detection process. Eight CSV files are created by the PFX analyzer, named out_B, out_Bx, out_By, out_Bz, out_E, out_Ex, out_Ey, and out_Ez. Each file has the same data structures as listed in Table 3.2. The purpose of these CSV files is for manual analysis by users; in addition, the files can be loaded by the PFX analyzer later on for reprocessing. Date Time contains the epoch of the observation point. LON contains the longitude of the geographic coordinates, LAT contains the latitude of the geographic coordinates, and ALT contains the altitude of the Akebono satellite when the Omega signal was detected at the observation point. The first series named NR, LB, HW, ND, LR, AZ, AS, and JP contains the estimation of intensity strength for each station; the second series contains the delay time of the Omega signal detection at the observation point.

Table 3.2 CSV file data structure created by PFX analyzer for manual analysis and reprocessing.

Field Name	Description
Date Time	Date and Time of the observation point
LON	Longitude in geographic coordinates
LAT	Latitude in geographic coordinates
ALT	Altitude of Akebono
NR	Detected intensity strength from Norway station
LB	Detected intensity strength from Liberia station
HW	Detected intensity strength from Hawaii station
ND	Detected intensity strength from North Dakota station
LR	Detected intensity strength from La Reunion station
AZ	Detected intensity strength from Argentina station
AS	Detected intensity strength from Australia station
JP	Detected intensity strength from Japan station
NR	Detected delay time from Norway station
LB	Detected delay time from Liberia station
HW	Detected delay time from Hawaii station
ND	Detected delay time from North Dakota station
LR	Detected delay time from La Reunion station
AZ	Detected delay time strength from Argentina station
AS	Detected delay time strength from Australia station
JP	Detected delay time strength from Japan station

3.3.3 Save and Load Map Files

The geomagnetic and geographic map results can be saved and loaded by the user. Table 3.3 shows the data structures of the Map files: in the Java programming language, these are stored as variables inside the GMap class and may be saved as class objects into a file and compressed with zip standard compression to reduce the size. GMap contains the estimated intensity strength or delay time for each region in geographic or geomagnetic coordinates. The number

of arrays indicates the longitude, latitude, altitude, MLT, and number of detected events. Stat contains the longitude and latitude location of the station in geographic coordinates; Stat2 contains the longitude and latitude location of the station in geomagnetic coordinates; Events_B contains the total number of detected events at a specific magnetic local time in the magnetic field; and Events_E contains the total number of detected events at a specific magnetic local time in the electric field.

Table 3.3 Data structure of the Map files. The files can be saved and loaded by the user for analytical purposes.

Field Name	Description
GMap [72][36][20][8][12]	Detected intensity strength or delay time
Stat [2]	Longitude and latitude in geographic coordinates
Stat2 [2]	Longitude and latitude in geomagnetic coordinates
Events_B [8]	Total detected events in the magnetic field
Events_E [8]	Total detected events in the electric field

The third tab window of the PFX analyzer displays the result of automatic detection on a geographic or geomagnetic map and interfaces to control the CSV and Map files, as illustrated in Figure 3.6. The top combo box contains eight selections of specific MLT and one station side that includes all MLT and restricts the result to only 10° to the east and west of the station. The left pane shows the control interfaces for the CSV and Map files. The combo box allows selection between intensity, delay time, and number of detected events. The list box displays eight station results and one result for all stations. Buttons |B| and |E| are used to load specific CSV files created by the PFX analyzer for reprocessing. The Load, Save, and Reset buttons are used for control of Map files. It is possible to load multiple Map or CSV files to combine results from multiple months or years.

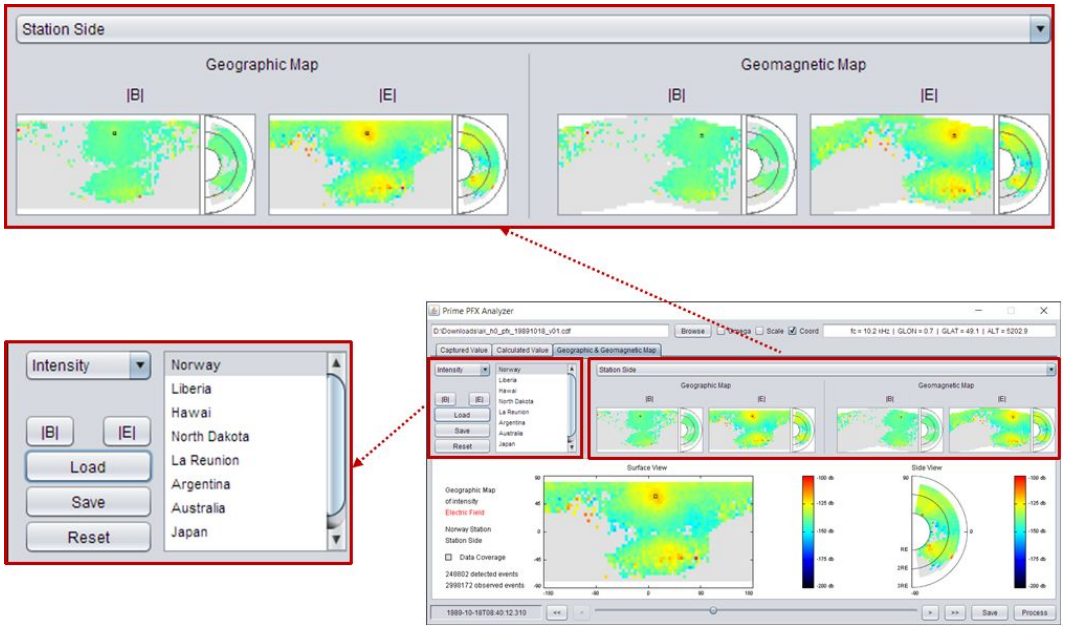

Figure 3.6 Results of automatic detection on a geographic or geomagnetic map and interfaces to control the CSV and Map files.

Chapter 4
Omega signal Propagation Analysis

4.1 Datasets

We first show the number of PFX data that we have processed in Figure 4.1. In the figure, we count one event which corresponds to 10 s duration of data when the center frequency of the PFX was fixed at 10.2 kHz. From October 1989 to September 1997, we measured 3,030,614 events in total. The number of events change every year. We obtained the highest number of events with 408,790 in 1992 and the lowest events with 213,155 in 1989. We also separated the datasets of events into four sides for the analysis based on magnetic local time (MLT). In the present study, we define dawnside, dayside, duskside and nightside as MLT from 3 to 9, from 9 to 15, from 15 to 21, and from 21 to 3, respectively. Comparing the number of events for each MLT or year, there are no significant difference except for data in 1989 because this year only contains data of three months. Therefore, the datasets coverage for each year and each MLT are reliable enough for the statistical analyses in this study.

Using these datasets, we can comprehensively analyze the Omega signals transmitted from each station. In the present paper, however, we analyzed signals transmitted from Norway and North Dakota stations located at high–middle-latitude region because the orbital condition of Akebono was suitable to detect the signals from these stations along the ambient magnetic field lines because of its elliptic and high inclination orbit.

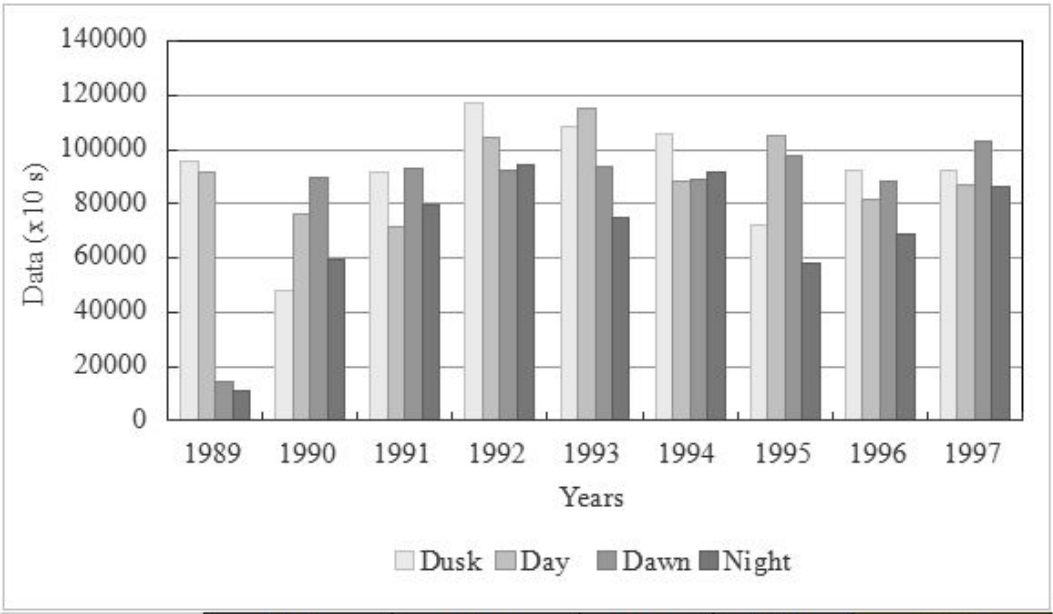

	Dusk	Day	Dawn	Night	Total
1989	95854	92003	14297	11001	213155
1990	48231	76448	89670	59446	273795
1991	91456	71240	92925	79300	334921
1992	117240	104322	92652	94576	408790
1993	108802	115379	93782	74649	392612
1994	105783	88317	88951	91894	374945
1995	72069	105293	97962	58127	333451
1996	92192	81758	88379	68660	330989
1997	92197	86643	102857	86259	367956
Total	823824	821403	761475	623912	3030614

Figure 4.1 Number of events processed from October 1989 to September 1997. Each event corresponds to 10 s duration of PFX data.

4.2 Event Study

To demonstrate the reliability of our datasets and the automatic detection, in this section we present result of study from few interesting events. Figure 4.2 (a) and 4.2 (b) shows 1.5 hours of trajectory of the Akebono from the northern to southern hemisphere from 08:29:39.802 UT to 09:55:33.842 UT on October 18, 1989. During this period, Omega signals from the Norway station were continuously observed and 344 signals were detected in the electric field and 63 signals were detected in the magnetic field. The location of the Norway station is

also shown as a small square in Figure 4.2 (a) and (b). The PFX data are not available between latitude 49°N to 26°N and 2°N to 6°S. This unavailable of data are shown as dashed lines in Figure 4.2 (a).

Figure 4.2 (c) shows absolute intensities of magnetic fields, Figure 4.2 (d) shows electric fields, and Figure 4.2 (e) shows delay time of the Omega signals. The red curves indicate moving median over 20 points (detected events). The intensity of the magnetic field and electric field of the Omega signal is showing higher intensity in the northern hemisphere where the Norway station was located. The Norway station was located at latitude 56.42°N, and we can see higher signal intensity approximately −283 dB (T) for the magnetic field and approximately −125 dB (V/m) for the electrical field. The intensity then becomes lower for the electric field or disappears for the magnetic field near the equator at latitude 0°. The signal for the electric field then increased at approximately −145 dB (V/m) near the southern hemisphere because the signal could propagate along the Earth's magnetic field. The delay time is around 0.2 s in the northern hemisphere where the Norway station was located and then increased to more than 0.5 s as the trajectory of the Akebono satellite got closer to the southern hemisphere. This occurred because propagation along the Earth's magnetic field required more time compared with a direct propagation path. Figure 4.2 (f) shows the approximate distance based on a simple magnetic dipole model for the propagation path of the signal along the Earth's magnetic field (Luhmann and Friesen, 1979; Prölss, 2004; Bayupati, 2012). The calculated distances was from the Norway station to the observation point.

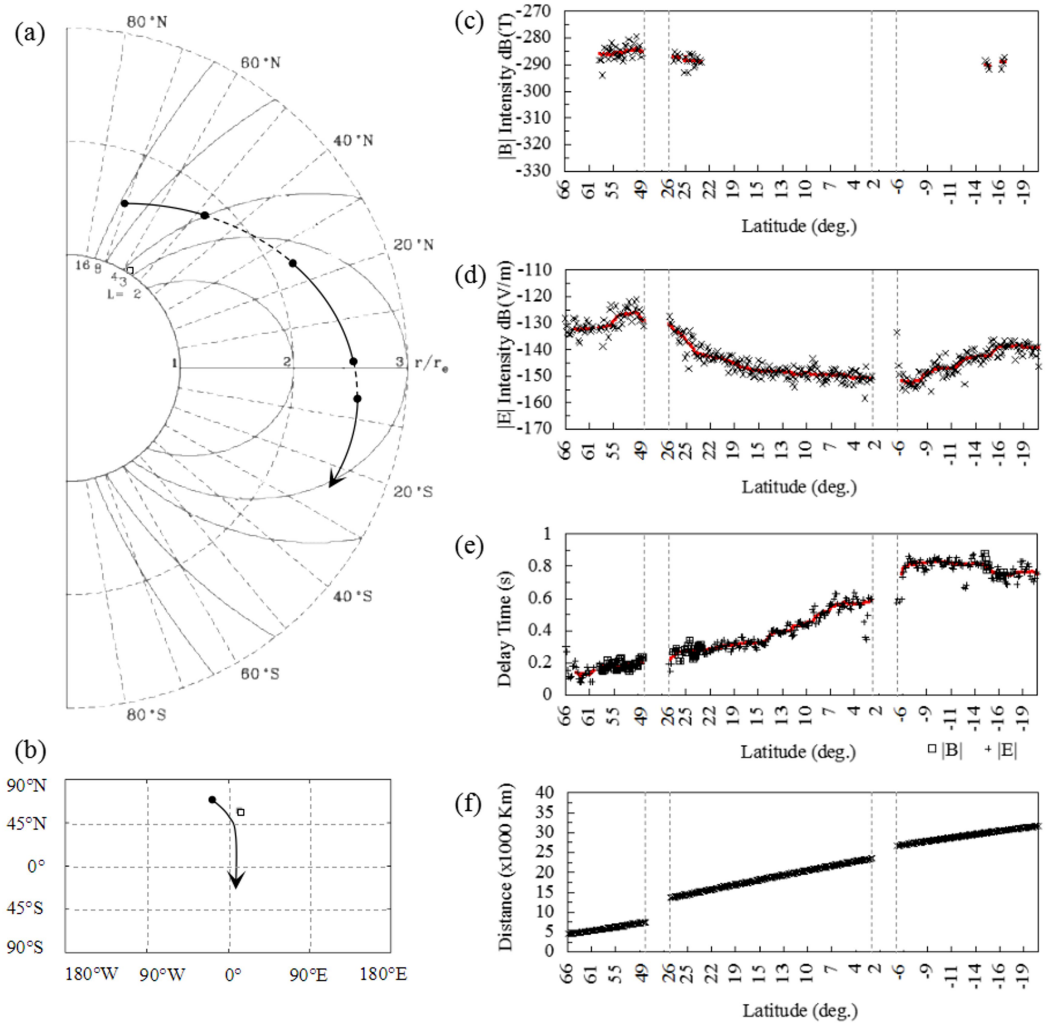

Figure 4.2 Trajectory of Akebono, and observed Omega signal of Norway station from 08:29:39.802 UT to 09:55:33.842 UT on October 18, 1989.

For comparison, we calculated the sliced center frequency of each signal in the Electric Field from 08:29:46 UT to 09:55:36 UT on October 18, 1989. We plotted only 1 bin (Δf = 10Hz/bin, Δt = ~9.4ms/bin) of the center frequency spectrum (~10.2 kHz) and arranged it as shown in the Figure 4.3. The transmission time of Norway station start at 08:29:46 UT and repeated every 10 seconds. We projected the red curves of trend line in Figure 4.2 (e) to Figure 4.3. This confirms that the automatic detection of our analyzer produced quite reliable results compared with manual analysis. Deviation occurred at few parts because of false result by multiple high intensity noises and affected moving median of the

trend line. Based on the Omega system transmission pattern, we expected signal from Norway should be 0.9 second in duration. Intensification at t=0.6 in a period from 08:29:46 UT to 08:57:46 UT was caused by the WIDA IC. Because of its weakness, WIDA IC may cause false intensification of signal as seen at t=2.05 in a period from 08:57:46 UT to 09:36:06 UT. These false signals repeat at the same time location for several minutes within 10 s duration of data and might appear again after 0.5 s from the previous false signal. The effects of WIDA IC can be seen clearly in Figure 2.4. Signal from Liberia station was expected to be delayed and might be received after t=1.0. In period from 09:36:06 UT to 09:55:36 UT, overlapped signal between Norway and Liberia is possible.

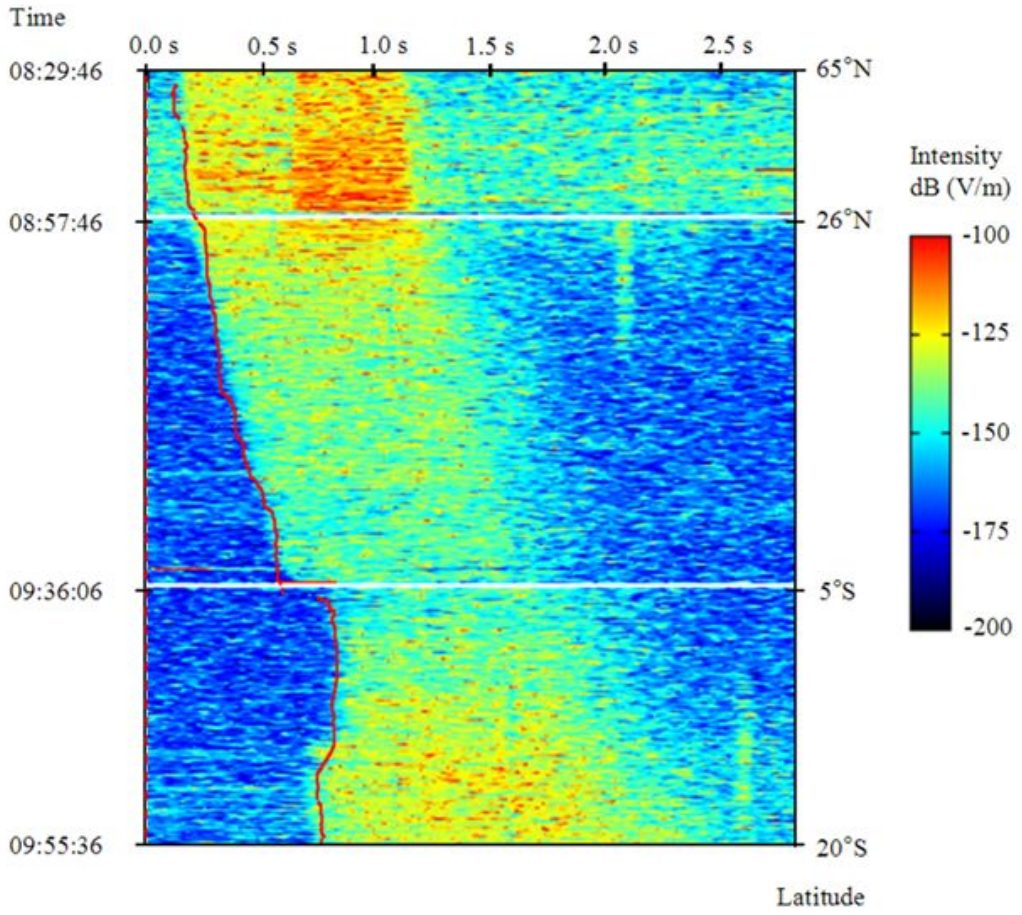

Figure 4.3 Sliced Center Frequency in the Electric Field from 08:29:46 UT to 09:55:36 UT on October 18, 1989. The transmission time of Norway station was 08:29:46 UT and repeated every 10 seconds. Signal from Norway expected to be 0.9 second in duration. Intensification at t=0.6 in a period from 08:29:46 UT to 08:57:46 UT was caused by the WIDA IC.

In Figure 4.4, we provided another PFX data that captured omega signal from North Dakota station. We plotted only 1 bin (Δf = 10Hz/bin, Δt = ~9.4ms/bin) of the center frequency spectrum (~10.2 kHz) and arranged it as shown in the Figure, where 1 bin represents 10 Hz in frequency resolution and ~9.4 ms in time resolution. The data start from 08:30:54 UT to 09:55:34 UT on October 18, 1989. The dashed red line is the transmission time of North Dakota station, that is start at the 15:53:49.6 and repeated every 10 s. There are unavailability of data between latitude of 11ºS to 43ºS . Another weakness of the WIDA IC can be seen in intensification of signal at t=3.1 and t=3.6 in a period from 15:53:49 UT to 16:38:29 UT.

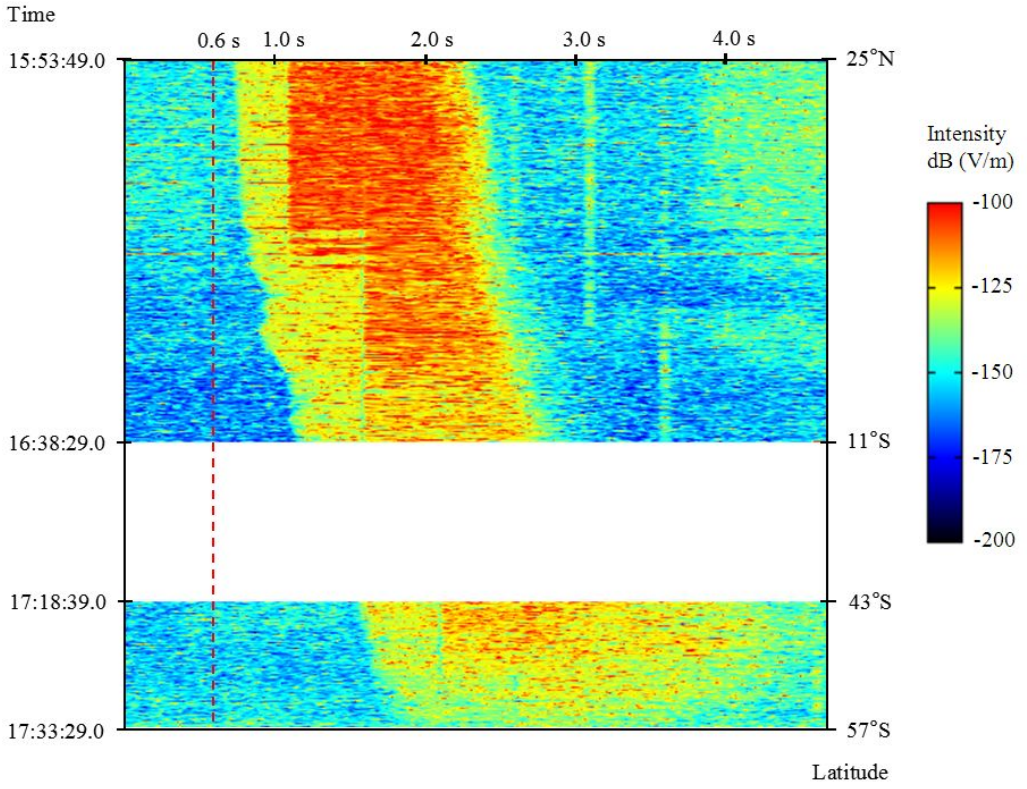

Figure 4.4 Sliced Center Frequency in the Electric Field from 15:53:49 UT to 17:33:29 UT on October 18, 1989.

4.3 General characteristics of Omega signal propagation from Norway and North Dakota Stations

First we study the signal intensity just above the transmission station to evaluate how wide and how much the Omega signals penetrated through the ionosphere over the station. For this purpose, we restricted the PFX data obtained below 640 km in altitude. Figure 4.5 (a) shows the number of events used for the analysis just above the Norway station from October 1989 to September 1997, which was located at longitude 100.72°E and latitude 55.96°N in geomagnetic coordinates. Figure 4.5 (b) and Figure 4.5 (c) show the averaged intensity of the signals in electric and magnetic fields, respectively. White areas on the map indicate unavailability of PFX data. The location of the station is shown on the map indicated by rectangle in each panel. We divided the horizontal axis into 20 bins of longitude (5° for each bin) and the vertical axis into 20 bins of latitude (5° for each bin). The gray color in Figure 4.5 (b) and Figure 4.5 (c) indicates no event was detected either because of the intensity too low if compared to the threshold level or because of high noise which made the condition of detection became false. The number of event in Figure 4.5 (a) and signal intensities in Fig 2 (b) and Figure 4.5 (c) are indicated by color scales given at the right of each panel. It is also notable that the high-intensity area was located at ~10° northern part of the transmitter station. The center of the penetration region is located approximately at longitude 97°E and latitude 65°N in geomagnetic coordinates. The intensities at this point were approximately −265 dB(T) in magnetic field and −120 dB(V/m) in electric field, respectively. It was also found that the region where Omega signal penetrated the ionosphere covered a radius of ~3,900 km from the center of the transmitter station, between approximately latitude 10°N to 80°N and longitude 70°E to 140°E in geomagnetic coordinates.

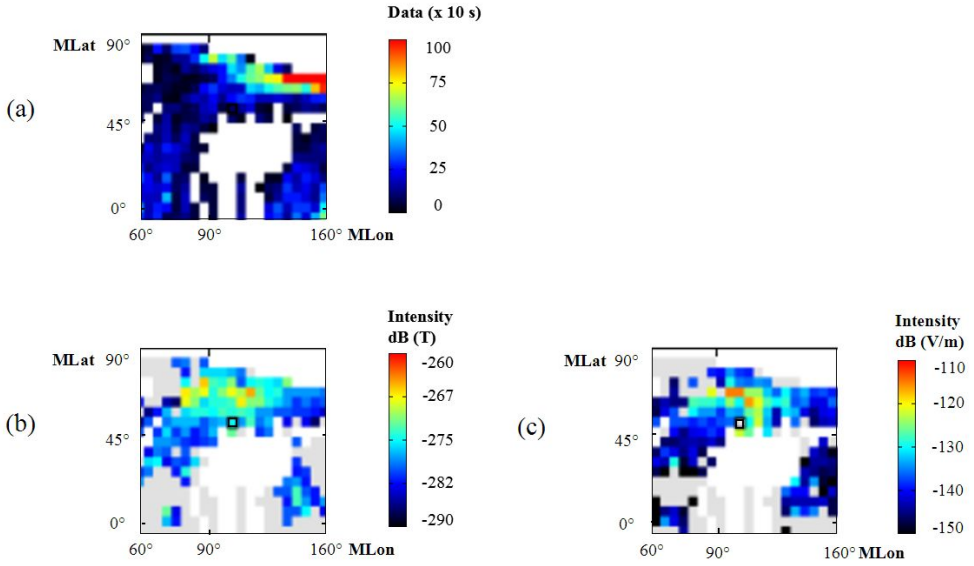

Figure 4.5 (a) Duration of data processed in the magnetic and electric field below altitude 640 km. (b) Omega signal propagation for the Norway station in the magnetic field and (c) the electric field. Rectangle indicates the location of Norway station at longitude 100.72°E and latitude 55.96°N.

As a next step, we investigated propagation characteristics of the Omega signal from Norway station at higher altitude region. In the analysis, we restricted the data measured between 10° to the east and 10° to the west in longitude from the transmitter station to illustrate the propagation of high intensity region with approximately 6 dB different between the center to the edge in the meridian plane. Figure 4.6 shows the Omega signal propagation pattern transmitted by the Norway station from October 1989 to September 1997 in geomagnetic coordinate. The rectangle on the map indicates location of the station (55.96°N). We plotted the meridian map into 20 bins of altitude (631.7 km for each bin) and 36 bins of latitude (5° for each bin). The highest-altitude PFX data that we have is under approximately 10,500 km; lowest-altitude PFX data available is above approximately 274 km. White areas on the map indicate unavailability of PFX data, especially around the equator below L<2, while more data is available at

higher altitude above 6371 km as shown in Figure 4.6 (a). The gray color in Figure 4.6 (b) and Figure 4.6 (c) indicates no event was detected in that region. In Figure 4.6 (b)(c), we can clearly find that the high intensities of the Omega signal from Norway station propagated along the Earth's magnetic field lines at a higher-latitude region, between 40°N and 80°N. The Omega signal in electric field did not attenuate as much as in magnetic field which attenuated completely below L<6; thus, it can be observed to have propagated higher, to 90°N. Furthermore, the propagation reached the opposite hemisphere between 40°S and 70°S in latitude.

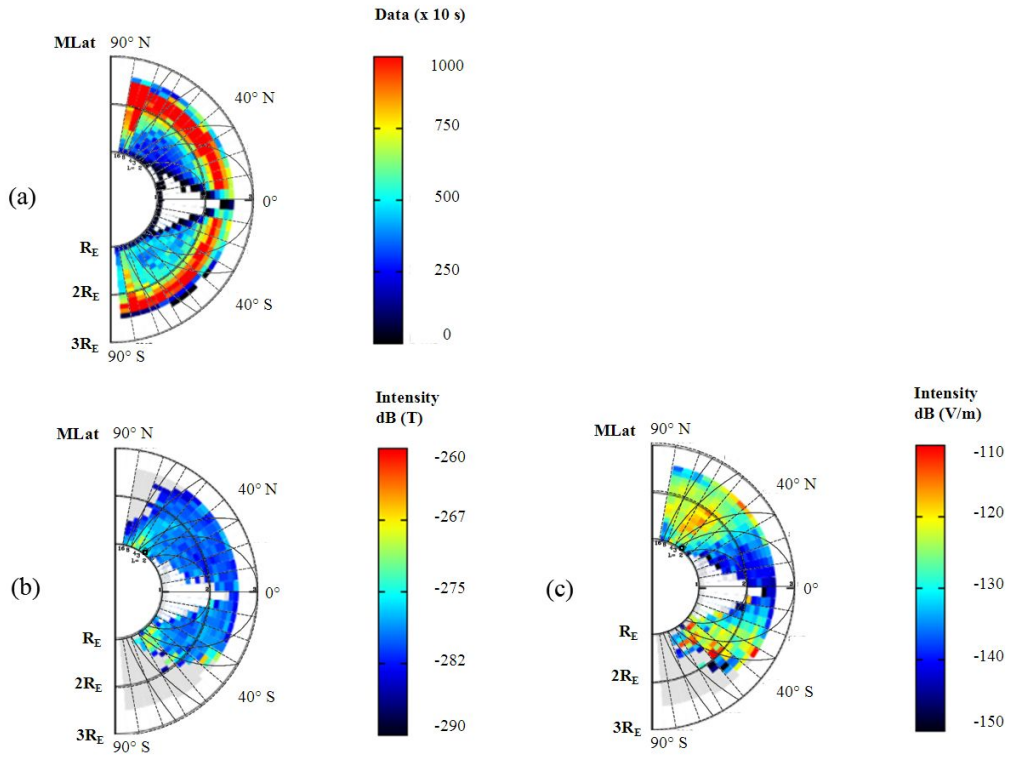

Figure 4.6 (a) Duration of data processed in the magnetic and electric field with longitude restricted to ±10°. (b) Omega signal propagation for the Norway station in the magnetic field and (c) the electric field. Rectangle indicates the location of Norway station at longitude 100.72°E and latitude 55.96°N.

Next, we show propagation characteristics of the Omega signals transmitted from North Dakota. It is important to note that the stations at Norway and North Dakota were located at the same latitude (55.9°N) in geomagnetic coordinates, but different latitude in geographic coordinates; the Norway station was located at 56.42°N, while the North Dakota station at 46.37°N in geographic coordinates.

Figure 4.7 (a) shows the number of events used for the analysis just above the North Dakota station from October 1989 to September 1997, which was located at longitude 34.83°W and latitude 55.98°N in geomagnetic coordinates. White areas on the map indicate unavailability of PFX data, especially around the eastern part of the transmitter station. Figure 4.7 (b) and Figure 4.7 (c) show the averaged intensity of the signals in electric and magnetic fields, respectively. The gray color indicates no event was detected in that region. The Omega signal that penetrated the ionosphere and propagated along the Earth's magnetic field lines covered a radius of ~3000 km in the region around the transmitter station between approximately latitude 10°N to 70°N and longitude 5°E to 65°W in geomagnetic coordinates. A high-intensity area is visible immediately above the station transmitter at approximately −255 dB(T) in the magnetic field and approximately −110 dB(V/m) in the electric field. Compared to the Norway station, different regions of high-intensity signal are apparent, where the center of the penetration region is located approximately at longitude 34°W and latitude 55°N in geomagnetic coordinates, despite both stations being at the same latitude in geomagnetic coordinates, approximately 55.9°N.

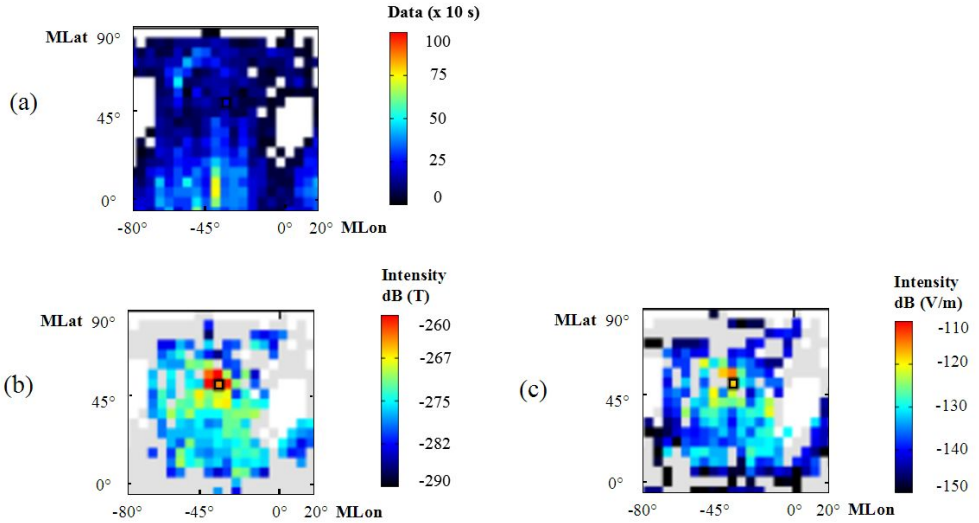

Figure 4.7 (a) Duration of data processed in the magnetic and electric field below altitude 640 km. (b) Omega signal propagation for the North Dakota station in the magnetic field and (c) in the electric field. Rectangle indicates the location of North Dakota station at longitude 34.83°W and latitude 55.98°N.

Figure 4.8 shows the Omega signal propagation pattern transmitted by the North Dakota station from October 1989 to September 1997 in geomagnetic coordinates with the same restrictions as Figure 4.6. The rectangle on the map indicates the location of the station (55.98°N). White areas on the map indicate unavailability of PFX data, especially below L<2 around the equator and L<3 in the southern hemisphere as shown in Figure 4.8 (a). The gray color in Figure 4.8 (b) and Figure 4.8 (c) indicates no event was detected in that region. As for the PFX data, more data is available at higher altitude above 6371 km however, in the southern hemisphere more data is also available below 6371 km as shown in Figure 4.8 (a). Compared to the Norway station, the high intensities of the Omega signal from the North Dakota station propagated at a lower-latitude region between 30° and 60°. Similarly to the Norway station, the Omega signal in the electric field did not attenuate as much as in the magnetic field which attenuated completely below L<5; thus, this signal was observed to propagate higher, to

90°N. Furthermore, the propagation reached the opposite hemisphere between 35°S and 65°S latitude.

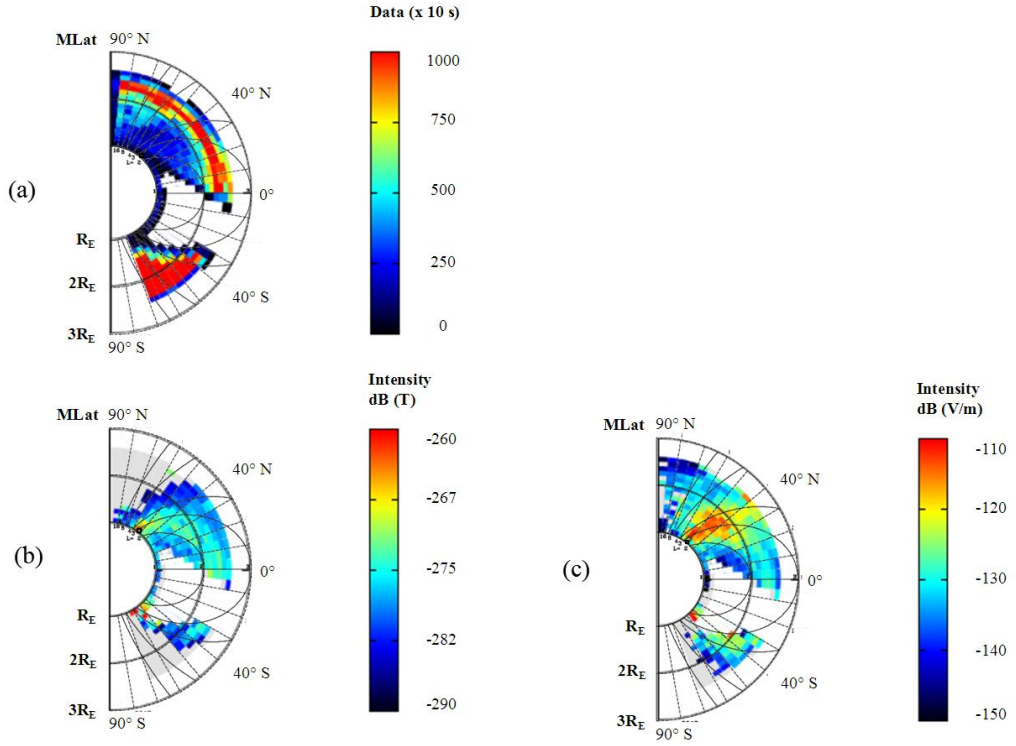

Figure 4.8 (a) Duration of data processed in the magnetic and electric field with longitude restricted to ±10°. (b) Omega signal propagation for the North Dakota station in the magnetic field and (c) in the electric field. Rectangle indicates the location of North Dakota station at longitude 34.83°W and latitude 55.98°N.

4.4 Magnetic Local Time Dependence

In this section, we examined the transmittance of Omega signals as a function of magnetic local time to evaluate the attenuation effect of the ionosphere and plasmasphere. Using the Magnetic Local Time (MLT) of the observation points, we separated the intensity maps every 3 hours. We compared the results using the data obtained around the Norway station and the North Dakota station. Figure 4.9 shows the Omega signal intensity transmitted by the Norway station from October 1989 to September 1997 in geomagnetic coordinate without any altitude data

restriction.The vertical axis indicates geomagnetic latitude and horizontal axis indicates geomagnetic longitude, and 8 panels correspond to the sections separated every 3 MLTs. For the longitude, it is centered at the location of the station with range of 100° (±50° centered at the station). The rectangle on the map indicates the location of the station which was located at longitude 100.72°E and latitude 55.96°N. The transition of the intensity level demonstrates that the nightside has a high intensity level at approximately −115 dB(V/m) in the electric field and approximately −265 dB(T) in the magnetic field. The dayside has the lowest intensity level, of approximately −120 dB(V/m) in the electric field and approximately −270 dB(T) in the magnetic field. In addition, the dayside (MLT 9-15) clearly exhibits narrow propagation with only ~50° width of range in longitude compared to the other MLT sides.

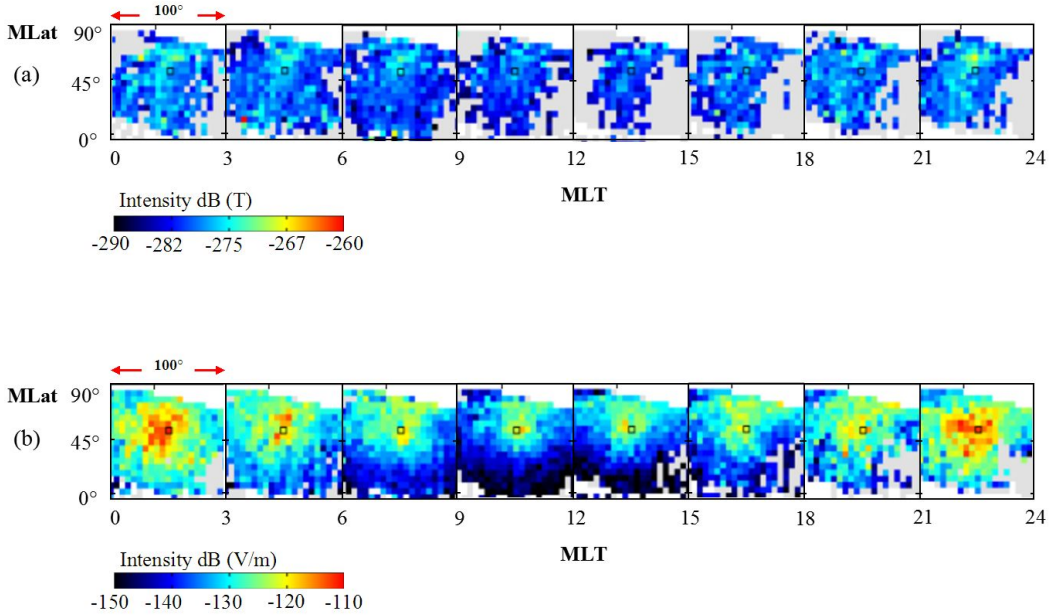

Figure 4.9 (a) Propagation of Omega signal from the Norway station based on local time in the magnetic field and (b) in the electric field. Red arrow indicates width of the map (~100°) with location of the station in the center which indicated by the rectangle.

Figure 4.10 shows the Omega signal propagation transmitted by the North Dakota station from October 1989 to September 1997 in geomagnetic coordinate without any altitude data restriction. The rectangle on the map indicates the location of the station which was located at longitude 34.83°W and latitude 55.98°N. The transition of the intensity level demonstrates that the nightside has a high intensity level at approximately −110 dB(V/m) in the electric field and around −265 dB(T) in the magnetic field. The dayside has the lowest intensity level of approximately −125 dB(V/m) in the electric field and approximately −270 dB(T) in the magnetic field. It is also apparent that the dayside (MLT 12-15) has narrow propagation in the magnetic field with only ~60° width of range in longitude compared to the other MLT sides. Comparing with the Norway station, the high-intensity regions are located around the southern part of the North Dakota station approximately at longitude 34°W and latitude 45°N; however, there is a similar transition in the propagation pattern between each MLT and the signals tend to propagate further in the nightside (MLT 21-3). If compared to the signals from Norway, the signals from North Dakota in nightside show higher level of intensity approximately 5 dB and wider high intensity region; however in dayside, it shows lower level of intensity approximately 5 db and narrower high intensity region.

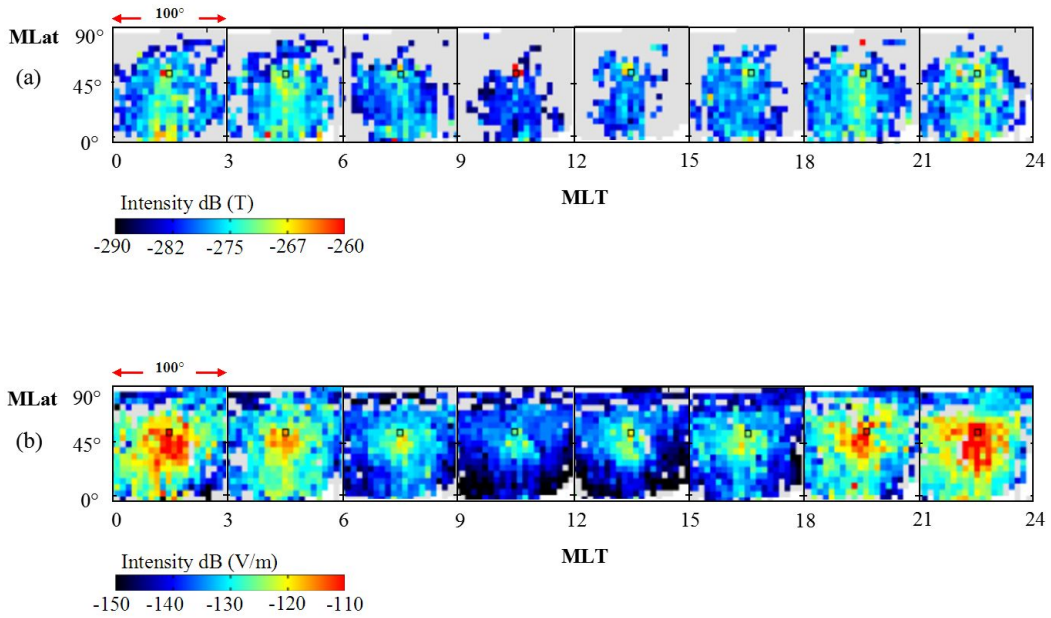

Figure 4.10 (a) Propagation of the Omega signal from the North Dakota station based on local time in the magnetic field and (b) in the electric field. Red arrow indicates width of the map (~100°) with the station in the center which indicated by the rectangle.

4.5 Seasonal Variation

In this section, we study the seasonal variation of Omega signals propagation to evaluate the trend of propagation characteristic for each season. In the analyses, we separated the eight years of data into four seasons centered at the equinox and solstice of each year. Data range for the March equinox is February 1 to April 30, June solstice is May 1 to July 31, September equinox is August 1 to October 31 and December solstice is November 1 to January 31.

Figure 4.11 shows the spatial distribution of Omega signals transmitted by the Norway station from October 1989 to September 1997. The vertical axis indicates geomagnetic latitude and horizontal axis indicates geomagnetic longitude. The rectangle on the map indicates the location of the station. Overall, the high-intensity region of the propagation was captured with an intensity level of approximately −270 dB(T) for the magnetic field and approximately −115 dB(V/m) for the electric field. Particularly, in the electric field, between June

solstice and December solstice, the high-intensity region was shifted ~10° toward the northern region of the transmitter station and the intensity in the southern region of the transmitter was decreased.

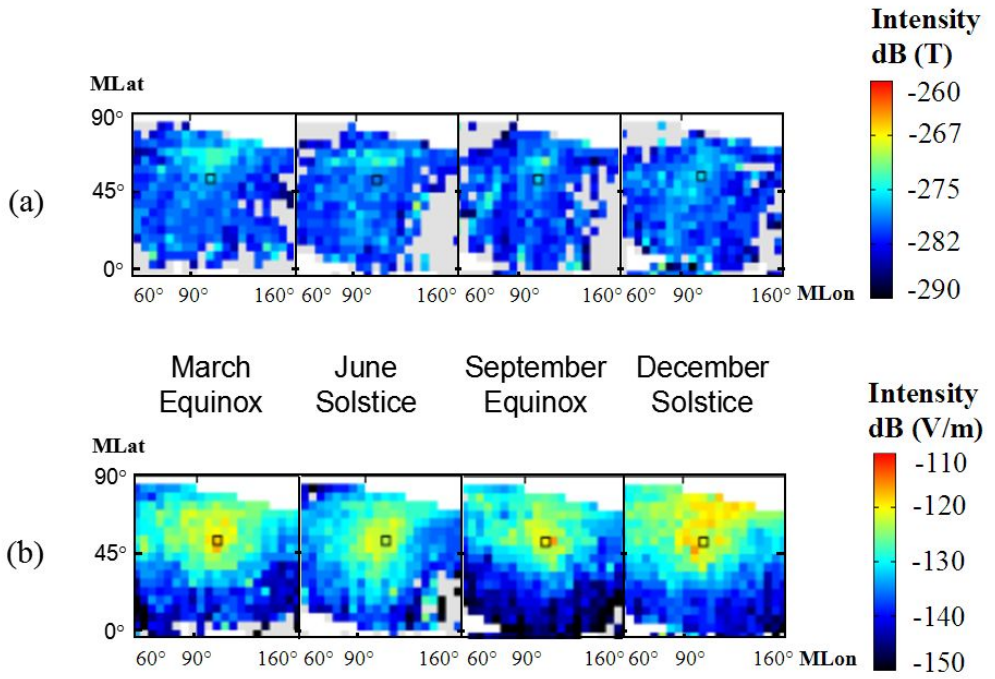

Figure 4.11 (a) Seasonal propagation of the Omega signal from the Norway station in the magnetic field and (b) in the electric field.

Figure 4.12 shows the spatial distribution of Omega signals transmitted by the Norway station from October 1989 to September 1997. The upper four panels show magnetic intensity and the lower four panels show electric intensity. As was shown in Figure 4.6, Omega signals tend to propagate along the geomagnetic field lines, we plot the intensity map taking its vertical axis as indicate invariant latitude (ILAT) of the observation point and the horizontal axis as geomagnetic longitude. The rectangle on the map indicates the location of the station. It was found that the high-intensity region was deviated 10° to higher invariant latitude from the transmitter. Intensities in the high-intensity region were approximately -275 dB(T) for the magnetic field and approximately -117 dB(V/m) for the electric field. Intense signals were detected in the wider region in December solstice, while the high-intensity region became the smallest in June solstice. In

addition, it is very interesting that, the high-intensity region in electric field was located only at 10° higher invariant latitude from the transmitter in June solstice. But it gradually spread northward (higher latitude) in September equinox and became the widest in December solstice. The region shrunk southward again in March equinox.

To understand the attenuation ratio between magnetic field and electric field based on the propagation distance from the Earth's surface, we show the magnetic and electric intensity distributions along the magnetic field lines in Figure 4.13 (a) and Figure 4.13 (b), respectively. The vertical axis indicates invariant latitude and the horizontal axis indicates distance from the Earth's surface along the magnetic field lines with maximum range of 12,742 km. Small red lines indicates latitude of the station location. We clearly see that the magnetic intensity attenuated gradually as the propagation distance became larger while electric intensity did not attenuate much even in the middle of distance at ~5700 km. In addition, signals tend to propagate within the narrower invariant latitude region in June solstice but they propagate wider invariant latitude region especially toward higher latitude region in December solstice and March equinox.

In Figure 4.13 (c) and Figure 4.13 (d), we show quantitatively standard errors of mean based on data from Figure 4.13 (a) and Figure 4.13 (b), respectively. It was calculated by using the standard deviation of all season data, and the standard error of all season data. The data only represent latitude of 10° higher than the station location to show the high intensity region. In the electric field, the minimum error is 0.8 dB and the maximum is 4.8 dB. In the magnetic field, the minimum error is 0.4 dB and the maximum is 2.9 dB. Furthermore, if we compare the attenuation ratio between the magnetic field and the electric field especially at middle distance of 6371 km, the magnetic field has higher ratio at 1.04 and the electric field is at ratio 0.94.

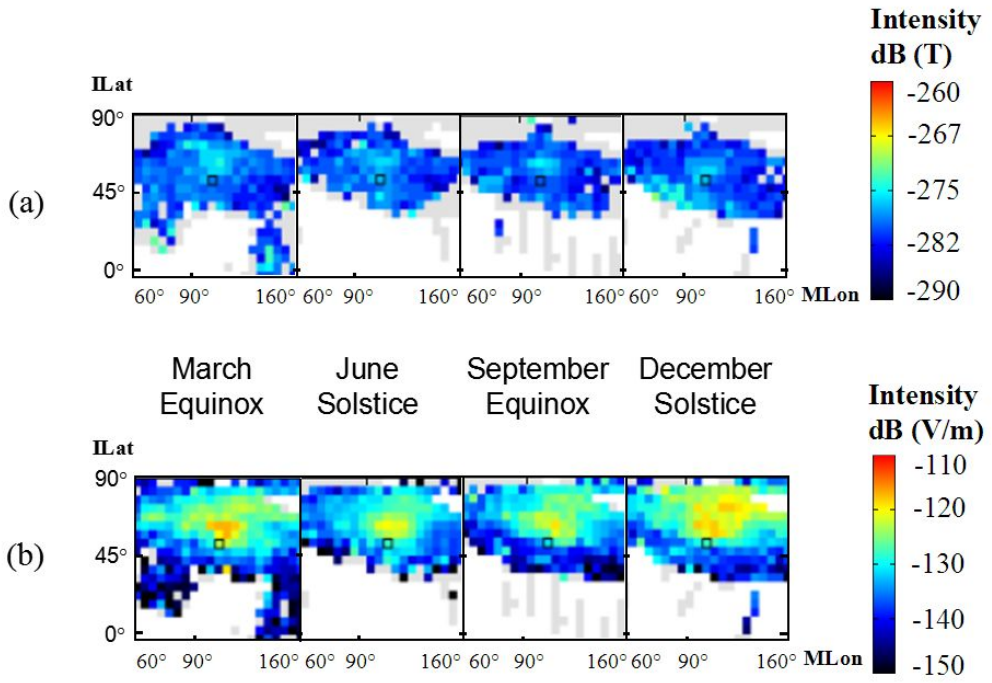

Figure 4.12 (a) Seasonal propagation of the Omega signal from the Norway station in the magnetic field and (b) in the electric field based on invariant latitude.

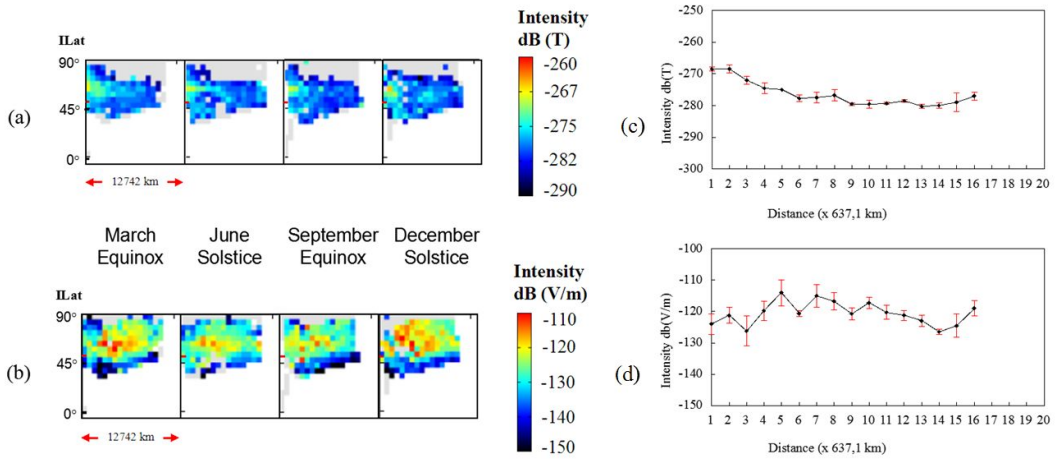

Figure 4.13 (a) Seasonal propagation of the Omega signal from the Norway station in the magnetic field and (b) in the electric field based on invariant latitude. (c) Median intensity and standard errors of mean of the seasonal propagation at 10° higher latitude from station location in the magnetic field and (d) in the electric field.

Figure 4.14 shows the spatial distribution of Omega signals transmitted by the North Dakota station from October 1989 to September 1997. The vertical axis indicates geomagnetic latitude and horizontal axis indicates geomagnetic longitude. The rectangle on the map indicates the location of the station. Overall, the high-intensity region of the propagation was captured at ~5° southern part of the station with an intensity level of approximately −265 dB(T) for the magnetic field and approximately −113 dB(V/m) for the electric field. Especially in the electric field, during the December solstice, this high-intensity propagation shifts to the region above the transmitter station and covers the northern region of the transmitter region. In the magnetic field, compared with the Norway station, the northern regions of the station show more attenuation at the September equinox and December solstice; however, this did not occur for the electric field.

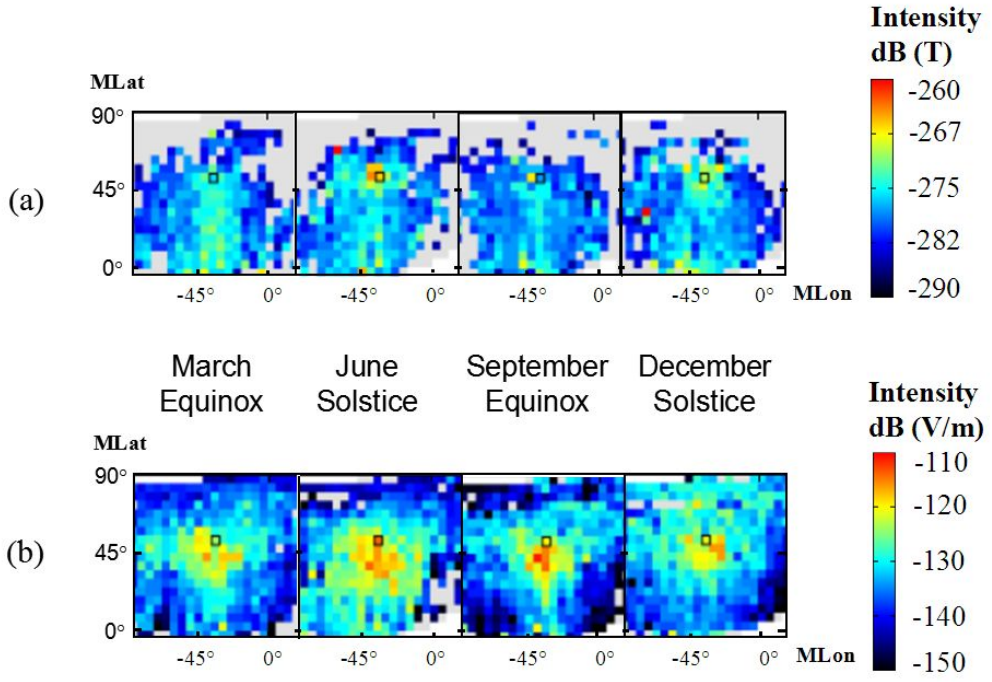

Figure 4.14 (a) Seasonal propagation of the Omega signal from the North Dakota station in the magnetic field and (b) in the electric field.

Figure 4.15 shows the spatial distribution of Omega signals transmitted by the North Dakota station from October 1989 to September 1997. The vertical axis

indicates invariant latitude (ILAT) of the observation point and horizontal axis indicates geomagnetic longitude. The rectangle on the map indicates the location of the station. We can also find that the high-intensity region of the propagation was deviated ~10° to higher latitude from the transmitter as in the Norway case (Figure 4.12). Intensities in the high-intensity region were approximately -270 dB(T) for the magnetic field and approximately -115 dB(V/m) for the electric field. Compared with the Norway case show in Figure 8, however, it is obvious that the high-intensity region was almost constant throughout the year and was not widely distributed even in December solstice. Figure 4.16 (a) and Figure 4.16 (b) show the magnetic and electric intensity distributions of Omega signals transmitted by the North Dakota station along the magnetic field lines. We also find that the Omega signals from the North Dakota tend to propagate along the ambient magnetic field lines within a limited invariant latitude. We assume that this happened because of the different geographic latitude even though the stations have the same geomagnetic latitude. That is, the Norway station was located at higher geographic latitude and thus Omega signals can propagate widely because of longer night in December solstice.

In Figure 4.16 (c) and Figure 4.16 (d), we show quantitatively standard errors of mean based on data from Figure 4.16 (a) and Figure 4.16 (b). The data represent latitude of 10° higher than the station location to show the high intensity region. In the electric field, the minimum error is 1.3 dB and the maximum is 14.1 dB. In the magnetic field, the minimum error is 0.3 dB and the maximum is 3.0 dB. Similar as in Norway case, if we compare the attenuation ratio between the magnetic field and the electric field especially at middle distance of 6371 km, the magnetic field has higher ratio at 1.03 and the electric field is at ratio 0.96.

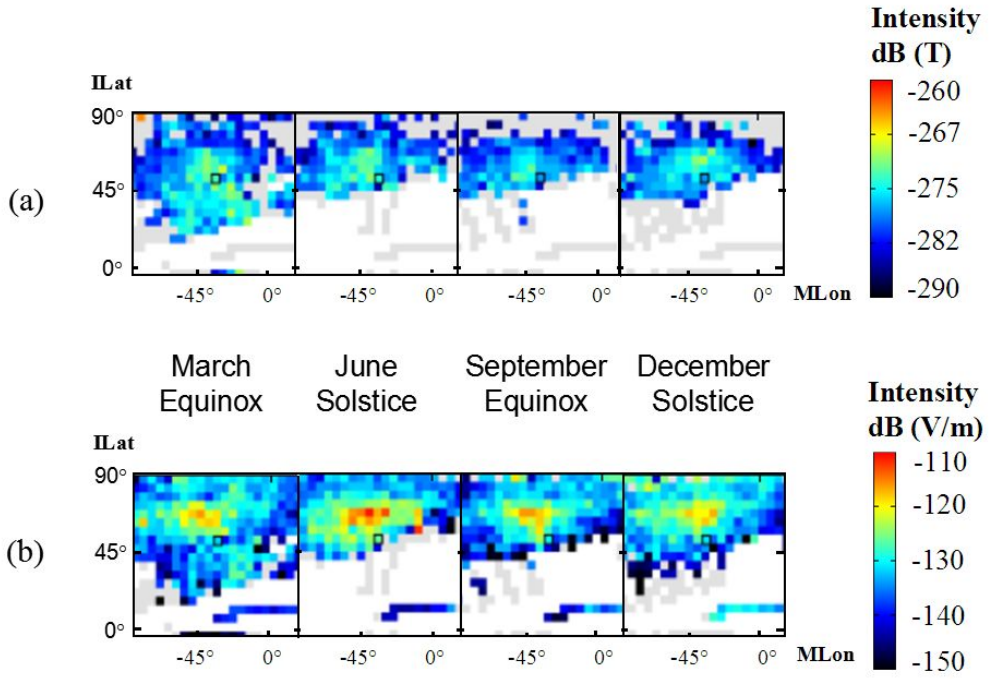

Figure 4.15 (a) Seasonal propagation of the Omega signal from the North Dakota station in the magnetic field and (b) in the electric field based on invariant latitude.

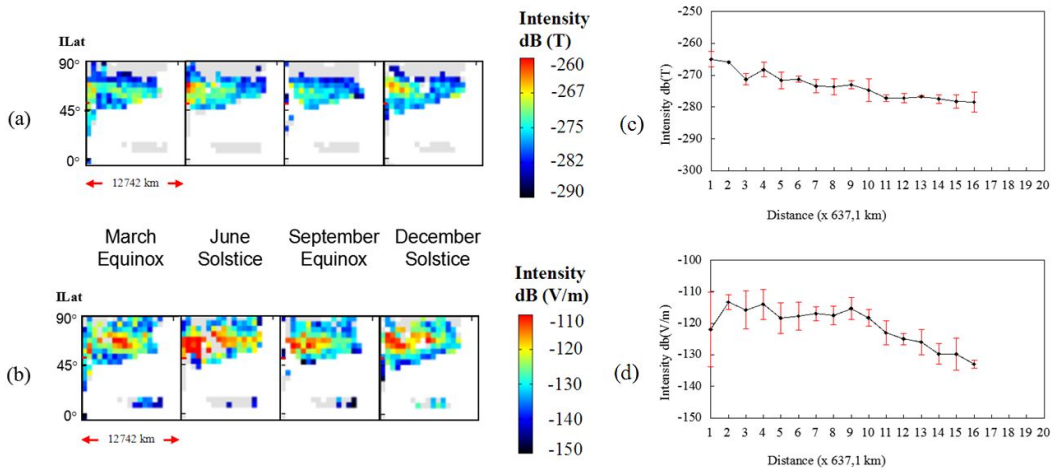

Figure 4.16 (a) Seasonal propagation of the Omega signal from the North Dakota station in the magnetic field and (b) in the electric field based on invariant latitude. (c) Median intensity and standard errors of mean of the seasonal propagation at 10° higher latitude from station location in the magnetic field and (d) in the electric field.

4.6 Annual Variation

Finally we study annual variation of propagation characteristics to evaluate the effects of solar activity. We separated the data and illustrated the results for each year. Figure 4.17 shows the Omega signal propagation pattern transmitted by the Norway station from October 1989 to September 1997 in geomagnetic coordinate. The vertical axis indicates geomagnetic latitude and horizontal axis indicates geomagnetic longitude with range of 100° (±50° centered at the station), and 9 panels corresponding to 1989 to 1997 are shown. The rectangle on the map indicates the location of the station. We used data below an altitude of 8200 km for the entire year because the satellite's altitude decreased every year and no data are available in 1997 above that altitude. Between 1989 and 1992, the intensity level was low; from 1993 to 1997, the average intensity level was higher and the propagation region of the Omega signal was wider. Based on sunspot cycle data (NASA/Marshall Solar Physics, 2016; Usoskin, 2008), the sunspots number on the surface of the sun increased between 1989 and 1992 during the solar maximum period, while it decreased between 1993 and 1997 corresponding to the solar minimum period. We demonstrate that solar activity significantly affected the propagation and penetration of Omega signal in the ionosphere. The Omega signal propagation intensity near the station during the solar maximum (1991) was approximately −280 dB(T) in the magnetic field and approximately −120 dB(V/m) in the electric field. During the solar minimum (1996), higher intensity level that propagated wider and farther from the transmitter station is apparent, approximately −270 dB(T) in the magnetic field and approximately −115 dB(V/m) in the electric field. Based on these maps, the coverage radius and intensity strength of the Omega signal that penetrated and propagated in the ionosphere altered by a few thousand kilometers every year.

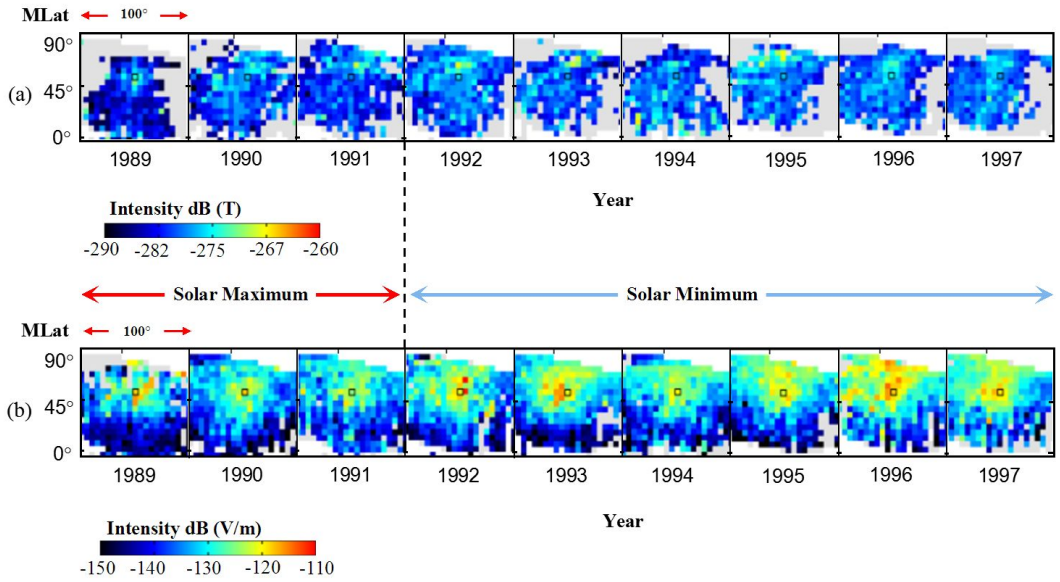

Figure 4.17 (a) Annual propagation of the Omega signal from the Norway station in the magnetic field and (b) in the electric field. Red arrow indicates width of the map (~100°) with location of the station in the center which indicated by the rectangle.

Chapter 5
Results and Discussion

5.1 Propagation in the Magnetic and Electric Fields

There are some other results that are interesting to be discussed in this chapter and related to future study. The results of eight years of data for the Norway station (October 1989–September 1997) are shown in Figure 5.1, plotted in geographic coordinates. The longitudinal axis consists of 72 bins of 5° for each bin; the latitudinal axis is 36 bins of 5° for each bin; and the altitudinal axis is 20 bins of 637.1 km for each bin. The rectangle on the map shows the location of the transmission station at longitude 13.14°E and latitude 56.42°N. Gray coloration on the map indicates areas for which PFX data were available, but no Omega signal was detected by the analyzer. White coloration on the map indicates that the PFX data are not available for that location. The meridian plane map shows the average intensity coverage of 10° to the east and 10° to the west from the station.

The intensity of the Omega signal in the electric field in Figure 5.1(b) does not attenuate along the propagation path compared to the magnetic field in Figure 5.1(a). In both figures, the Omega signal can be observed to propagate to the southern hemisphere along the Earth's magnetic field. The intensity of the signal near the equator shows a low intensity at high altitude and no signal at lower altitude. We concluded that this unique propagation is caused primarily by the location of the transmission station, the Earth's magnetic field, and the global

electron density. A previous study of global electron density had analyzed the normal wave direction and delay time of the Omega signal (Kimura et al., 1997). For eight years (96 months), we observed 83,696 detected signals in the magnetic field and 262,085 detected signals in the electric field.

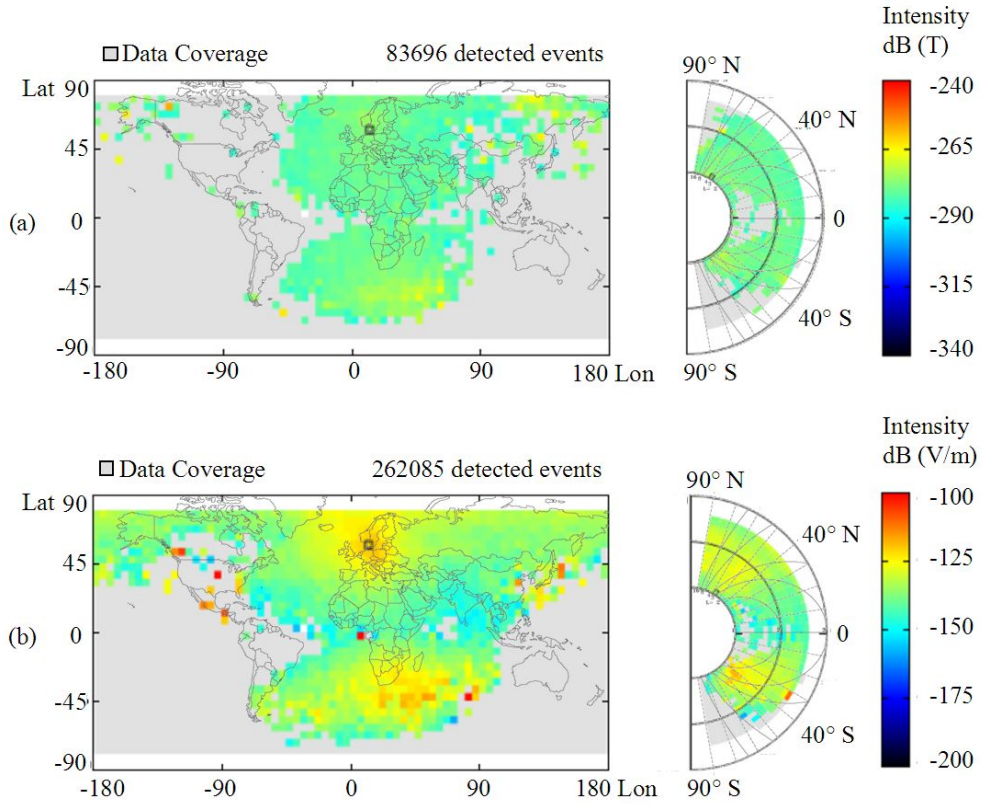

Figure 5.1 Omega signal propagation of the Norway station from October 1989 to September 1997 in the magnetic field (a) and the electric field (b). The Omega signal propagated to the southern hemisphere along the Earth's magnetic field. Near the equator, the signal shows low intensity at high altitude and no signal at lower altitude.

5.2 Intensity Map and Delay Time Map for All Stations

In this section, all-station intensity maps in both geographic and geomagnetic coordinates are described and discussed. From the information displayed in the maps, it is clear that the global propagation trend was affected by the global

electron density and location effects of the stations. From October 1989 to September 1997, we observed 127,900 detected signals in the magnetic field and 476,134 detected signals in the electric field. The intensity map for all stations in geographic coordinates is displayed in Figure 5.2. We provide an actual land map on the figure for informational purposes, and all the station locations are indicated by rectangles with abbreviations. Figure 5.3 contains a station intensity map in geomagnetic coordinates. Compared to the geographic map, the data appear curved because of the bearing with respect to the magnetic poles. In the meridian plane map, high-intensity regions can be observed to propagate along the Earth's magnetic field lines.

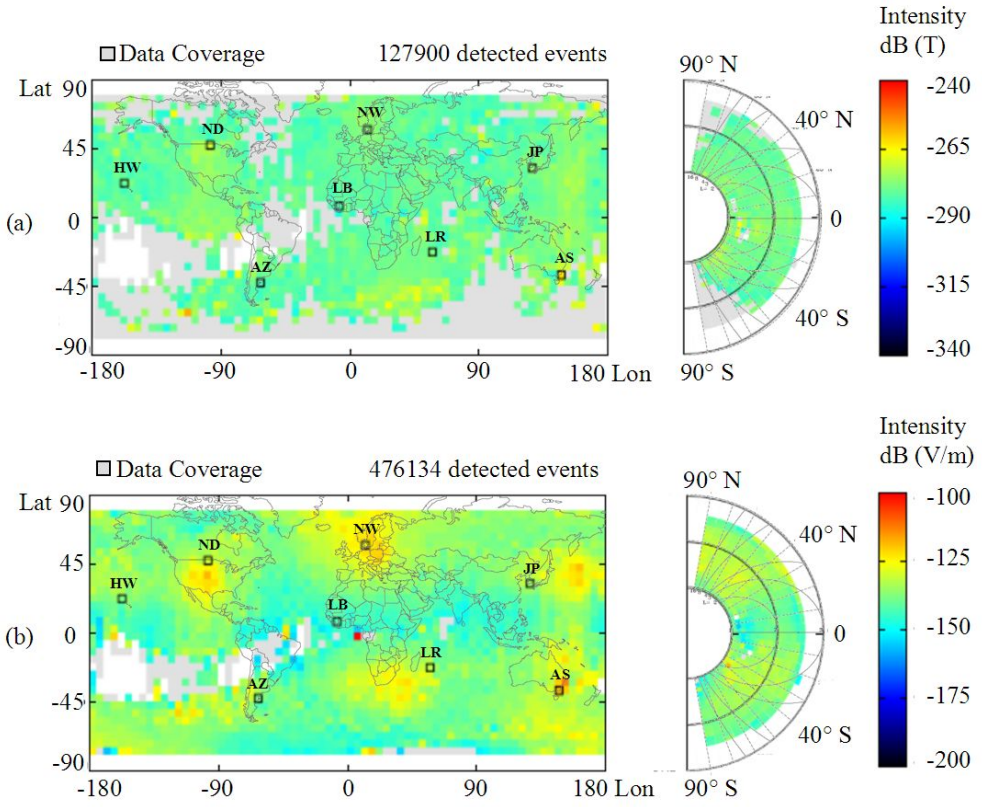

Figure 5.2 All-station intensity map in geographic coordinates from October 1989 to September 1997 in the magnetic field (a) and in the electric field (b).

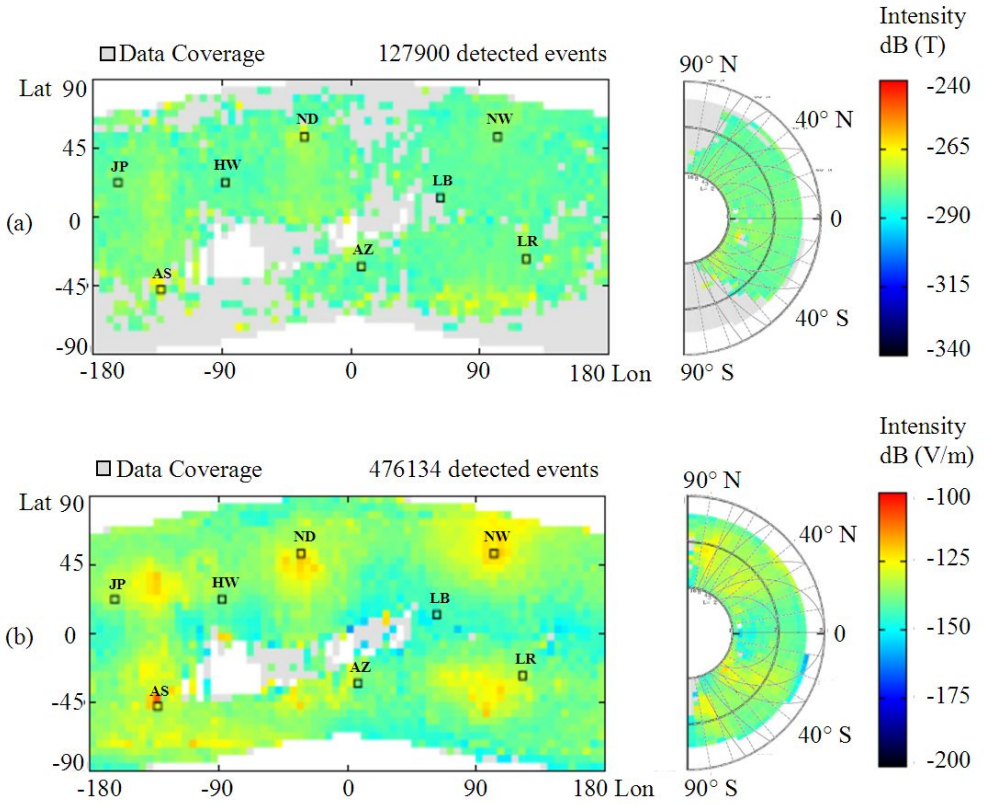

Figure 5.3 All-station intensity map in geomagnetic coordinates from October 1989 to September 1997 in the magnetic field (a) and in the electric field (b).

High–middle-latitude stations show high intensity of the Omega signal in a wide area of propagation from its transmitter compared to the low-latitude stations. The all-stations delay time maps show an interesting trend, indicated by red dashed curves in Figure 5.4, which indicate the boundaries between low and high delay time. We assume that the electron density is greater near the equator compared to that near the poles. This trend may be caused by the fluctuation of solar radiation directly affecting the electrons along the Earth's magnetic field lines. Further investigation is required to confirm this interesting trend and determine the correlation behind it.

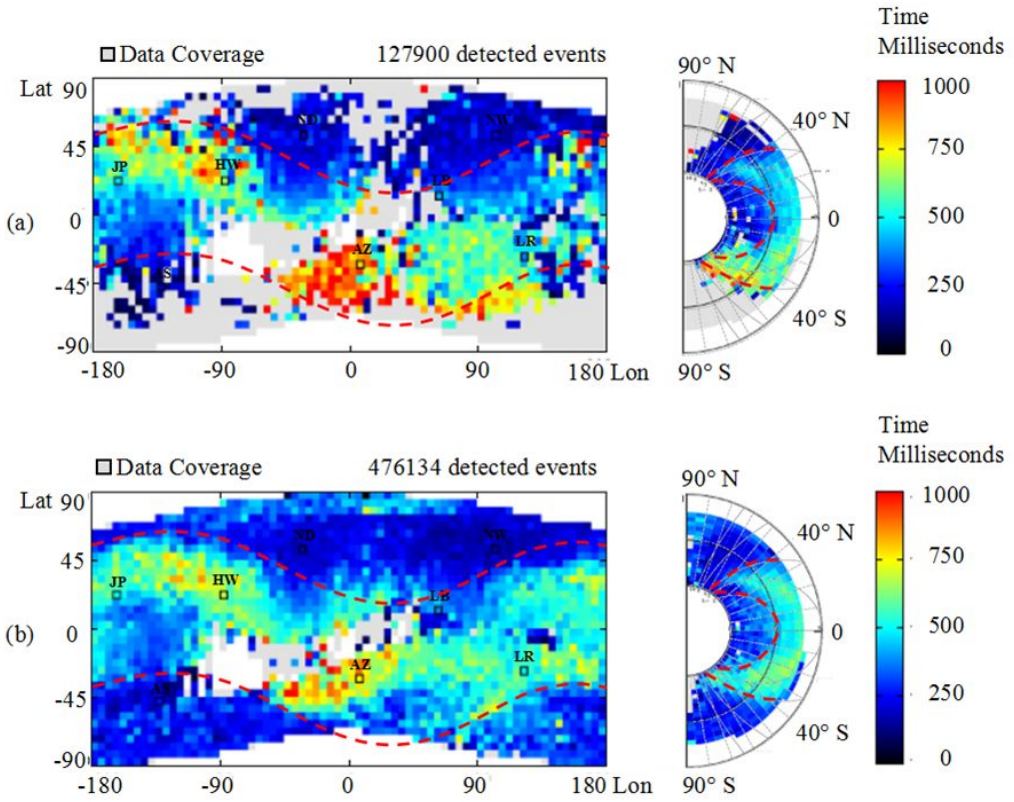

Figure 5.4 All-station delay time map in geomagnetic coordinates from October 1989 to September 1997 in the magnetic field (a) and in the electric field (b).

Chapter 6
Concluding Remarks

In this study, we developed an advanced detection algorithm for continuous processing of large amounts of data measured for several years by the PFX subsystem on board the Akebono satellite. The algorithm enables us to distinguish noise and real Omega signals and detect errors in order to produce more accurate results. Compared to manual analysis, automatic detection can be accomplished with short periods of processing time and does not require human intervention in the process.

We studied the high–middle-latitude Omega stations located at Norway and North Dakota and evaluated how wide and how much the Omega signals penetrated through the ionosphere over the station. Our analysis revealed that, for stations located at almost the same latitude in geomagnetic coordinates, the Omega signal propagated along the Earth's magnetic field differently. Omega signals transmitted from both stations tended to propagate along the geomagnetic field lines and reached to the opposite hemisphere. But the signals from Norway propagated in the higher latitude region compared to the one from North Dakota. This phenomenon resulted from the different latitude location of the station in geographic coordinates, in which the Norway station was located at 56.42°N and the North Dakota station at 46.37°N. Because of this geographic difference, we suggest that effect of attenuation ratio in the ionosphere worked differently. We will discuss this point in more detail later.

Second we examined the transmittance of Omega signals as a function of magnetic local time to evaluate the attenuation effect of the ionosphere and plasmasphere. We found that the Omega signal tended to propagate farther in the nightside, where the electron density in the ionosphere was lower than in the dayside. This result is consistent with the previous studies by Collier et al. [2006] and Oike et al. [2014], in which they studied the occurrence frequencies of lightning whistlers. Collier et al. [2006] demonstrated that detection frequency of lightning whistlers on the ground were higher at night than daytime. On the other hand, Oike et al. [2014] studied the lightning whistlers detected in the plasmasphere and showed that the occurrence frequency was maximum after sunset. Oike et al. [2014] suggested that this is caused by the combination of occurrence frequency of lightning and attenuation effect of the ionosphere. That is, the occurrence frequency of lightning itself is peaked at late afternoon but the attenuation ratio is smaller at night, then the detection peak on the spacecraft become maximum after sunset. In case of the ground measurement, it is necessary to penetrate the ionosphere twice and thus lightning whistlers tend to be detected at night on the ground. In that sense, our statistical study is valuable to evaluate the attenuation ratio of VLF waves in the ionosphere quantitatively.

As for the propagation characteristics in the plasmasphere, we showed that the signal intensity in magnetic field gradually decrease along the propagation path, while the attenuation ratio in electric field is lower and the signals can propagate more widely and farther to the other hemisphere from the original transmission station. This tendency suggests that the wave changed from electromagnetic to electrostatic as it propagates in the plasmasphere with its wave normal deviated from the ambient magnetic field line.

We also studied on the seasonal variation of Omega signals to evaluate the trend of propagation characteristic. We found that intense signals from Norway station were detected in the wider region in December solstice, while the

high-intensity region became the smallest in June solstice. But the signals from North Dakota did not widely distributed and they tended to propagate narrower region along the ambient magnetic field. This is probably because the Norway station was located at higher geographic latitude and thus the duration of night was expected to be longer compared to that of the North Dakota station in December solstice, so that the signals from the Norway station did not attenuated in December solstice and propagated widely in the higher latitude region.

Finally, we studied the annual variation of the propagation characteristics of Omega signals to evaluate the effects of solar activity. We found that in 1991, when solar activity was at a maximum, the Omega signal propagated at a lower intensity level; in contrast, in 1996 when solar activity was at a minimum, the Omega signal propagated at a higher intensity level and farther from the transmitter station. We assumed that plasmaspheric electron density and temperatures affected the propagation of the Omega signal.

As was described in the introduction, quantitative study of the Omega signals using the eight years of PFX data from October 1989 to September 1997 is quite important to evaluate the attenuation ratio of VLF waves propagating in the ionosphere and plasmasphere as a function of magnetic local time, season, annual solar activity. In the future, extensive study of the delay time and wave normal direction are necessary to clarify the global features of the ionosphere and plasmasphere quantitatively.

Acknowledgment

There are many people I would like to express my deep gratitude while I was pursuing Doctoral degree in Japan. First of all, my supervisor in Kanazawa University Prof. Yoshiya Kasahara. Despite of his busy works yet very kindly spared his time and power for guidance in completion of my research in his lab. He has been sharing some of his knowledge and idea to improve the quality of my research and carefully planning all the stages of my research progress from lectures, advises in meeting, conferences, journal submissions, and finally completion of my dissertation. I also feel pleasure to his presence and friendliness during our leisure in several lab's event outside the research context. Moreover, I was very glad that he accepted me as his student when I was applying my doctoral research proposal to Kanazawa University.

I would like to thank Dr. Yoshitaka Goto, who has been contributes his time in supporting the completion of my research and also gave some comments and suggestions to improve my research. He also very friendly whenever we had the chance for conversation.

I would like to thank all of the family members of Communication and Information Engineering Lab. Since the first time I joined the lab, even with language difficulty, some of the members have been interacting and supporting me to complete my research. My deepest gratitude to Mr. Keisuke Shima who was my tutor and Mr. Ryota Watanabe, they helped me a lot in my first year in Japan to handle all of the administration requirement related to university, apartment and city hall. Also Mr. Yuta Oike, Mr. Shoya Matsuda, Mr. Mamoru Ota, Mr. Win Zaw

Hein, other doctoral students who supported my research and really good conversation partners whenever we have the chance to chat.

I would like to thank Prof. Satoshi Yagitani for sharing his knowledge in lecture and always give warm greetings every time we met. Dr. Mitsunori Ozaki and all Prof. Yagitani's Laboratory members who always enliven our meeting and parties. Also Prof. Masato Miyoshi, Prof. Masahiro Mambo, Dr. Hidetaka Nambo for sharing their knowledge in lecture and enlightened me with many worthwhile learning.

I would like to express my gratitude to Indonesian government, which provided scholarship to Japan. I am very grateful chosen as one of the scholarship awardee and without such financial support, I would not be able to come to Japan and pursue my Doctoral degree.

I also would like to thank Mr. Putu Agung Bayupati for his recommendation to Prof. Yoshiya Kasahara's lab and shared knowledge related to the research before I came to Japan. Also to all of my colleagues and staffs in Information Technology Department of Udayana University who supported me before and after I came to Japan and also Indonesian students community for all the events and interactions in Kanazawa.

I also would like to thank Kanazawa University Kyudo club for all the fun and relaxing time. Experiences in the club are priceless and I feel the feeling of being young Japanese peoples in their traditional culture and customs, also befriended many Japanese and learn many things.

The data used in this study were provided by the Akebono Project which was conducted by JAXA, Japan.

Bibliography

Bayupati, P.A., 2012. Study on Dispersion of Lightning Whistlers Observed by Akebono Satellite in the Earth's Plasmasphere (Doctoral dissertation).

Carpenter, D.L., 1963. Whistler evidence of a 'knee' in the magnetospheric ionization density profile, J. Geophys. Res., 68, 1675–1682.

Chi, P.J., et al. , 2013. Sounding of the plasmasphere by Mid-continent MAgnetoseismic Chain (McMAC) magnetometers, J. Geophys. Res. Space Physics, 118, 3077–3086, doi:10.1002/jgra.50274.

Collier, A. B., A. R. W. Hughes, J. Lichtenberger, and P. Steinbach (2006), Seasonal and diurnal variation of lightning activity over southern Africa and correlation with European whistler observations, Ann. Geophys., 24, 529–542.

Crouchley, J., 1964. A study of whistling atmospherics, *Aust. J. Phys, 17,* 88-105.

Ganguly, S., V. Wickwar , and J.M. Goodman, 2001. New generation topside sounder , Radio Science, 36, 5, 167-1179.

Goto, Y., Y. Kasahara, T. Sato, 2003. Determination of plasmaspheric electron density profile by a stochastic approach, Radio Science, 38(3), 1060, doi:10.1029/2002RS002603.

Helliwell, R. A. , 1965. Whistlers and Related Ionospheric Phenomena, Stanford Univ. Press, Stanford, Calif.

Kasahara, Y., 1995. Study on ELF/VLF Emissions in a Multicomponent Plasma Oberved by the Akebono Satellite (Doctoral dissertation).

Kimura, I., 1966. Effects of Ions on Whistler-Mode Ray Tracing, Radio Science, 1, pp.269-283.

Kimura, I., K. Hashimoto, I. Nagano, T. Okada, M. Yamamoto, T. Yoshino, H. Matsumoto, M. Ejiri, K. Hayashi, 1990. VLF Observation by the Akebono (EXOS-D) Satellite, Journal of Geomagnetism and Geoelectricity, 42, pp. 459-478.

Kimura, I., Y. Kasahara, H. Oya, 2001. Determination of global plasmaspheric electron density profile by tomographic approach using Omega signals and ray tracing, Journal of Atmospheric and Solar-Terrestrial Physics, 63, 1157–1170.

Kotova, G., V. Bezrukikh, M. Verigin, and J. Smilauer, 2004. In situ observations of low-density regions inside the plasmasphere, Earth Planets Space, 56, 989–996.

Lichtenberger, J., C. Ferencz, L. Bodnar, D. Hamar, and P. Steinbach, 2008. Automatic whistler detector and analyzer system: Automatic whistler detector, J. Geophys. Res., 113, A12201, doi:10.1029/2008JA013467.

Luhmann, J. G., and L. M. Friesen, A simple model magnetosphere, 84, 4405-4408, 1979.

Menk, F., Z. Kale, M. Sciffer, P. Robinson, C. Waters, et al., 2014. Remote sensing the plasmasphere, plasmapause, plumes and other features using ground-based magnetometers. J. Space Weather Space Clim., 4, A34, 2014, DOI: 10.1051/swsc/2014030.

Morris, P. B., R. R. Gupta, R. S. Warren, P. M. Creamer, 1994. Omega Navigation System Course Book, Vol. 1, National Technical Information Service, Springfield, Virginia, 434pp.

NASA/Marshall Solar Physics, 2016. http://solarscience.msfc.nasa.gov/SunspotCycle.shtml

Oike, Y., Y. Kasahara, and Y. Goto, 2014. Spatial distribution and temporal variations of occurrence frequency of lightning whistlers observed by VLF/WBA onboard Akebono, Radio Sci., 49, 753–764, doi:10.1002/2014RS005523

Prölss, G. W., 2004. Physics of the Earth's space environment: an introduction, Springer.

Pulinets, S.A., et al., 2001. MIR Space Station Topside Sounding near Taiwan, TAO, Vol. 12, No. 3, 525-536.

Reinisch, B.W., X. Huang, 2001. Deducing topside profiles and total electron content from bottomside ionograms, Advances in Space Research, 27, 1, 23-30.

Sandel, B.R., R.A. King,W.T. Forrester , D.L. Gallagher, A.L. Broadfoot, and C.C. Curtis, 2001. Initial results from the IMAGE Extreme Ultraviolet Imager, Geophys. Res. Lett., 28(8), 1439–1442.

Sandel, B.R., J. Goldstein, D.L. Gallagher, and M. Spasojevic, 2003. Extreme ultraviolet imager observations of the structure and dynamics of the plasmasphere, Space Sci. Rev., 109, 25–46.

Sawada, A., T. Nobata, Y. Kishi, I. Kimura, 1993. Electron Density Profile in the Magnetosphere Deduced From in Situ Electron Density and Wave Normal Directions of Omega Signals Observed by the Akebono (EXOS D) Satellite, Journal of Geophysical Research, 98, A7, 11267-11274.

Singh, R., A. K. Singh, and R. P. Singh, 2003. Synchronized whistlers recorded at Varanasi, Pramana Journal of Physics, 60, no.6, 1273-1277.

Suarjaya, I.M.A.D., Y. Kasahara, Y. Goto, 2016. Automatic Detection of Omega Signals Captured by the Poynting Flux Analyzer (PFX) on Board the Akebono Satellite, International Journal of Advanced Computer Science and Applications, 7(10), 67-74, doi:10.14569/IJACSA.2016.071009

Tarcsai, G., P. Szemeredy, and L. Hegymegi (1988), Average electron density profiles in the plasmasphere between L = 1.4 and 3.2 deduced from whistlers, J. Atmos. Terr. Phys., 50(7), 07–611, doi:10.1016/0021-9169(88)90058-X.

Usoskin I.G., 2008. A History of Solar Activity over Millennia. Living Reviews in Solar Physics 5 (3). doi:10.12942/lrsp-2008-3.